ALMA MATER STUDIORUM
UNIVERSITÀ DI BOLOGNA

ARCHIVIO ISTITUZIONALE
DELLA RICERCA

Alma Mater Studiorum Università di Bologna
Archivio istituzionale della ricerca

Intra-tumoral copper modulates PD-L1 expression and influences tumor immune evasion

This is the final peer-reviewed author's accepted manuscript (postprint) of the following publication:

Published Version:
Intra-tumoral copper modulates PD-L1 expression and influences tumor immune evasion / Voli, Florida; Valli, Emanuele; Lerra, Luigi; Kimpton, Kathleen; Saletta, Federica; Giorgi, Federico M; Mercatelli, Daniele; Rouaen, Jourdin R C; Shen, Sylvie; Murray, Jayne E; Ahmed-Cox, Aria; Cirillo, Giuseppe; Mayoh, Chelsea; Beavis, Paul A; Haber, Michelle; Trapani, Joseph A; Kavallaris, Maria; Vittorio, Orazio. - In: CANCER RESEARCH. - ISSN 0008-5472. - ELETTRONICO. - 80:19(2020), pp. 4129-4144. [10.1158/0008-5472.CAN-20-0471]

Availability:
This version is available at: https://hdl.handle.net/11585/777521 since: 2020-11-03

Published:
DOI: http://doi.org/10.1158/0008-5472.CAN-20-0471

Terms of use:

Some rights reserved. The terms and conditions for the reuse of this version of the manuscript are specified in the publishing policy. For all terms of use and more information see the publisher's website.

This item was downloaded from IRIS Università di Bologna (https://cris.unibo.it/).
When citing, please refer to the published version.

(Article begins on next page)

25 April 2024

Intra-tumoral copper modulates PD-L1 expression and influences tumor immune evasion.

Florida Voli [¥1,2], Emanuele Valli [¥1,2], Luigi Lerra[1], Kathleen Kimpton[1,3], Federica Saletta[1,4], Federico M. Giorgi[5], Daniele Mercatelli[5], Jourdin R.C. Rouaen[1], Sylvie Shen[6], Jayne E. Murray[1], Aria Ahmed-Cox[1], Giuseppe Cirillo[7], Chelsea Mayoh[1,2], Paul A. Beavis[8], Michelle Haber[1], Joseph A. Trapani[8], Maria Kavallaris*[1,2,3] and Orazio Vittorio*[1,2,3]

[1] Children's Cancer Institute, Lowy Cancer Research Centre, UNSW Sydney, Randwick, NSW 2031, Australia.

[2] School of Women's and Children's Health, UNSW Sydney, Sydney, Australia.

[3] ARC Centre of Excellence in Convergent Bio-Nano Science and Technology, Australian Centre for NanoMedicine, UNSW Sydney, NSW, Sydney, Australia

[4] Children's Cancer Research Unit, Kids Research Institute, The Children's Hospital at Westmead, Westmead, NSW 2145, Australia

[5] Department of Pharmacy and Biotechnology, University of Bologna, Bologna, 40126, Italy.

[6] Cord & Marrow Transplant Facility, Kids Cancer Centre, Sydney Children's Hospital, Sydney, Australia

[7] Department of Pharmacy, Health and Nutritional Sciences, University of Calabria, Rende, Italy

[8] Rosie Lew Cancer Immunology Program, Peter MacCallum Cancer Centre, Melbourne, Australia

***** Corresponding authors

[¥] Authors equally contributed

Running Title: Copper levels influence the expression of PD-L1 in tumors

Keywords: PD-L1, Copper, Cancer, Immune evasion, CTR-1.

Financial support for each author:

OV: National Health and Medical Research Council (NHMRC) Career Development Fellowship (APP1164960); Cure Cancer Australia, Priority-driven Collaborative

Cancer Research Scheme (APP 1141582); Cancer Institute NSW Career Development Fellowship (RG161875); Tour de Cure Grant; The Ross Trust Foundation.

MK: National Health and Medical Research Council (NHMRC) Program Grant (APP1091261; NHMRC Principal Research Fellowship (APP1119152); ARC Centre of Excellence in Convergent Bio-Nano Science and Technology (CE140100036).

MH: National Health and Medical Research Council (NHMRC) Program Grant (APP1091261); Cancer Institute New South Wales (CINSW) Program Grant (14/TPG/1-13).

Corresponding authors:

Orazio Vittorio, M. Sc, PhD, Scientia Fellow UNSW & NHMRC CDF

Senior Lecturer at the School of Women's and Children's Health UNSW

Children's Cancer Institute, Lowy Cancer Research Centre, UNSW, PO Box 81

Randwick NSW 2031 Australia

Phone: 02 9385 1557 Email: OVittorio@ccia.unsw.edu.au

Professor Maria Kavallaris, AM FAHMS FRSN, Head, Translational Cancer Nanomedicine Theme, NHMRC Principal Research Fellow

Children's Cancer Institute, Lowy Cancer Research Centre, UNSW, PO Box 81

Randwick NSW 2031 Australia

Phone: +61 2 9385 2151 Email: m.kavallaris@ccia.unsw.edu.au

Conflict of interest: The authors have declared that no conflict of interest exists.

ABSTRACT

Therapeutic checkpoint antibodies blocking PD1/PD-L1 signaling have radically improved clinical outcomes in cancer. However, the regulation of PD-L1 expression on tumor cells is still poorly understood. Here we show that intra-tumoral copper levels influence PD-L1 expression in cancer cells. Deep analysis of the TCGA database and TMA showed strong correlation between the major copper influx transporter CTR-1 and PD-L1 expression across many cancers but not in corresponding normal tissues. Copper supplementation enhanced PD-L1 expression at mRNA and protein levels in cancer cells and RNAseq revealed that copper regulates key signaling pathways mediating PD-L1-driven cancer immune evasion. Conversely, copper chelators inhibited phosphorylation of STAT3 and EGFR and promoted ubiquitin-mediated degradation of PD-L1. Copper-chelating drugs also significantly increased the number of tumor-infiltrating CD8+T and natural-killer cells, slowed tumor growth, and improved mouse survival. Overall, this study reveals an important role for copper in regulating PD-L1 and suggests that anti-cancer immunotherapy might be enhanced by pharmacologically reducing intra-tumor copper levels.

STATEMENT OF SIGNIFICANCE

Findings characterize the role of copper in modulating PD-L1 expression and contributing to cancer immune evasion, highlighting the potential for repurposing copper chelators as enhancers of antitumor immunity.

INTRODUCTION

Cancer immune evasion is recognized as a central hallmark of tumor development. One mechanism that cancer cells use to protect themselves from anti-tumor immune responses is over-expression of Programmed Death Ligand 1 (PD-L1). The immune checkpoint protein Programmed Death receptor 1 (PD-1) expressed by lymphocytes negatively regulates T-cell effector functions, leading to reduced cytokine production and cytotoxic activity against target cells, including tumor cells (1). Several therapeutic monoclonal antibodies targeting PD-L1/PD-1 have been approved by the FDA for adult melanoma and lung cancer (2). However, their efficacy, particularly for PD-L1/PD-1 blockade, is limited by cancer cell resistance in many patients (3) and immune-related adverse events in others (4). There is a need to better understand the mechanisms regulating the PD-L1/PD-1 axis to augment approaches that target this pathway.

Copper (Cu) homeostasis is finely regulated in mammals and Cu imbalance is associated with pathologies as diverse as Wilson's disease (severe Cu overload) or, as recently demonstrated, cancer susceptibility (5). Cu is essential for key signaling pathways that govern at least three key properties of malignant cells: proliferative immortality, angiogenesis, and metastasis. Although copper levels in cancer tissue is known to be highly heterogeneous, elevated Cu content has been reported in a wide spectrum of cancers including neuroblastoma (NB) (6), glioblastoma (GBM) (7), breast, ovarian, lung, prostate, stomach and leukemia (5), highlighting Cu homeostasis as an emerging therapeutic target in oncology. Interestingly, Cu also plays an important role in maintaining normal immunity, but its mechanism of action has not been determined (8). Early reports showed that dietary depletion of Cu increases the susceptibility of mice to bacterial pathogens (8). However, there are no

studies investigating a potential role for Cu in regulating anti-tumor immune responses.

Given the high levels of Cu in cancer, and the previously reported role of Cu in regulating immune cell function, our aim was to understand how elevated intra-tumoral Cu levels modulate the molecular pathways responsible for cancer immune evasion. In the present study, we describe a role for Cu in regulating the expression of PD-L1 in cancer cells, and we demonstrate that Cu chelating drugs have the potential to be repurposed for immune-checkpoint blockade therapy.

MATERIAL AND METHODS

Patient cohort Immunohistochemistry (IHC)

The retrospective patient cohort consisted of 180 patients (90 neuroblastoma and 90 brain tumor cases) who underwent diagnostic biopsy or surgical resection at the Children's Hospital at Westmead, Sydney, Australia (Human Ethics approval LNR /13 /SCHN /389). In the tissue microarrays (TMAs) each sample was present at least in duplicate.

Immunohistochemistry staining and image analysis

IHC was performed using a BOND-RX automatic immunostainer (Leica Biosystem). The slides were scanned using an Aperio CS2 virtual microscope (Leica Biosystem). The slides were incubated with CTR-1 antibody (Abcam, ab133385 1:100 dilution), with PD-L1 antibody (ab80276 1:50 dilution), with MT1X antibody (Proteintech #17172-1-AP 1:100 dilution) and with phospho-EGFR antibody (Cell Signaling #3777 1:100 dilution). The percentage of tumor cells showing positive membrane staining

was determined and the intensity of staining was judged on a semiquantitative scale of 0 to 3: no staining (0), weakly positive staining (1), moderately positive staining (2), and strongly positive staining (3). The H-score was derived as the product of the percentage of positive cells and the staining intensity to produce a score out of 300. Staining for CD3, CD4 and CD8 was used to estimate the cell density of tumor-infiltrating T-lymphocytes, while CD16, CD244 and CD335 staining was used to estimate the density of infiltrating NK cells. Staining for CD25 and FOXP3 was used to estimate the density of T regulatory cells.

Statistical analyses of immunohistochemistry staining

Statistical analyses were undertaken using SPSS version 22.0 (SPSS Inc.). Bivariate relationships between CTR-1-positive and PD-L1-positive cases were analyzed using cross tabulation and the association between expression was determined using Pearson correlation coefficient (Phi coefficient) while significance was tested using Fisher's exact test.

Student's t-test was carried out for independent samples among untreated and Dextran-Catechin treated (at 24 and 48h) Th-MYCN derived neuroblastoma tumors for PD-L1 and CTR-1 H-score, as well as immune cell density. Similarly, Student's t-test was used to compare Th-MYCN derived neuroblastoma tumors untreated or treated with TEPA for the expression of PD-L1 as well as the presence of infiltrating immune cells. Statistical significance was set at $p<0.05$.

Cell lines

Neuroblastoma cell lines SK-N-BE(2)-C, SK-N-FI, SH-SY5Y and glioblastoma cell line U87MG were obtained from ATCC and maintained in DMEM (Thermo Fisher

Scientific) with 10% FBS. All cell lines were validated by PCR (STR profiling) at the Children's Cancer Institute and routinely screened for Mycoplasma species.

Chemicals

Dextran-Catechin (DC) was synthesized and characterized as previously described (9). Tetraethylenepentamine pentahydrochloride (TEPA, cat#375683), copper chloride hydrate ($CuCl_2$, cat#C3279), Gefitinib (EGFR tyrosine kinase inhibitor, cat#SML1657) and MG-132 (proteasome inhibitor, cat#M7449) were purchased from Sigma-Aldrich. Interferon-gamma (IFNγ) was purchased from Roche (cat#11040596001).

***In vitro* drug treatment**

Cells were seeded in tissue-culture treated 6-well plates for 24 h before addition of freshly diluted drug in a final volume of 1mL (DC at 20μg/mL, TEPA at 2mM, $CuCl_2$ at 1mM and IFNγ or control). Cells were harvested after 24h of treatment with DC, TEPA. Treatment with 1 mM of $CuCl_2$ were performed up to 8 h, whereas the dose response experiments with 20μM, 50 μM, 100 μM and 200 μM of $CuCl_2$ were performed at 24h of incubation. Cells were incubated with IFNγ up to 4h before being harvested and proteins were extracted. To study the effect of copper chelators on EGFR phosphorylation cells were seeded in tissue-culture treated 6-well plates for 24 h before addition of freshly diluted drug in a final volume of 1mL (DC at 20μg/mL, TEPA at 2mM and Gefitinib 10μM) and incubated for 24h. Drugs concentrations and incubation times were optimized to keep cells viable.

Gene expression analysis

Real-time PCR (qPCR) analysis was performed using a SsoAdvanced Universal SYBR Green Super-mix (Bio-rad, cat #172-5270) and the CFX96 Real-time system (Bio-rad). Quantifications were normalized using endogenous control GUSB. *MT1X* (F: GCTTCTCCTTGCCTCGAAAT and R: GCAGCAGCTCTTCTTGCAG), *GUSB* (F: TGGTGCGTAGGGACAAGAAC and R: CCAAGGATTTGGTGTGAGCG), *PD-L1* (F: TTGTGGATCCAGTCACCTCTG and R: TTGATGGTCACTGCTTGTCC) primers were used in qPCR.

Immunoblotting

Cells were washed with cold PBS then lysed using scrapers in cold RIPA buffer (Thermo Scientific, cat #89901) containing protease inhibitors and phosphatase inhibitors. Quantification of proteins was conducted using a Pierce BCA protein assay kit (Thermo Scientific, cat #23225). Protein samples were mixed with 4X Laemmli buffer (Bio-Rad, cat #161-0747, containing β-mercaptoethanol). Protein electrophoresis of whole cell lysates (15-30 µg) or tumor lysates (60µg), was analyzed by Western blot.

siRNA gene silencing

The siRNA oligonucleotides used for silencing CTR-1 were purchased from QIAGEN (cat#1027416) and were Hs-CTR1 cat #SI042273045 (siRNA#1) and Hs-CTR1 cat #SI04936512 (siRNA#2). Control cells were transfected with a scrambled siRNA duplex (QIAGEN, cat#1027280), which has no homology with any other human mRNAs. SK-N-FI cells were seeded in tissue-culture treated 6-well plates at $2.5x10^5$ and they were transfected with Lipofectamine LTX Transfection Reagent (Qiagen, cat#P/N94756) with 20 nM siRNA. After 6h, media was diluted with fresh

DMEM+10%FCS. Cells were harvested 24h post-transfection and analyzed by Western blot.

For co-culture experiments with NK cells, SK-N-FI cells were seeded in tissue-culture treated 96-well plates at $5x10^3$ and transfected with LTX Transfection Reagent (Qiagen) with 20 nM siRNA. After 6h from transfection, media was diluted with fresh DMEM+10%FCS. 48h post-transfection, media was replaced with a ratio of 1:1 with NK cells (in NK media) and incubated for a maximum of 6h. Finally, NK cells were removed, and live cancer cells were counted by Trypan-blue exclusion.

Inductively Coupled Plasma Mass Spectrometry (ICP-MS)

SH-SY5Y at 7 $x10^5$, SK-N-FI at 6.5 $x10^5$, SK-N-BE(2)-C at 5.5 $x10^5$ and U87MG cells at 5.5 $x10^5$ were seeded in $25cm^2$ flasks and grown in DMEM media with 10% FBS for 24 hours. The following day, the cells were treated with DC at 20µg/mL or transfected with siRNA for CTR-1 (20nM siRNAs) for 24 hours or with copper at 1mM for 1h and 4h. Cells were then lysed with scrapers using milli-Q water, incubated at least 10 minutes in ice. A small amount (5%) of lysate was saved for protein quantification. Samples were supplied in 15mL falcon tubes to Mark Wainwright Analytical Centre, at UNSW, Australia. Samples were then open digested with 2% nitric acid solution. Samples were analyzed by ICP-MS using NexION 300D with Universal cell technology (Perkin Elmer, USA).

RNA-sequencing

SH-SY5Y cells at 2.5 $x10^5$ were seeded in tissue-culture treated 6-well plates and left growing for 24h before addition of freshly diluted drug (DC, TEPA, $CuCl_2$ and IFNγ) or control. Cells were harvested after 24h of drug treatment for DC, TEPA and

IFNγ or after 4h of $CuCl_2$. RNA was also extracted from tumors excised from Th-MYCN mice. 30 mg of tumor tissue was homogenized. RNA was isolated using RNeasy mini kit (Qiagen, cat#74104). DNA contamination was removed by performing on-column DNase digestion (Qiagen, cat #79254). Quality control and library preparation were carried out by Ramaciotti Centre for Genomics (UNSW, Australia). Paired-end 100bp sequencing was performed on the Illumina NovaSeq 6000 using TruSeq stranded mRNA for a total of 1.6B reads.

Bioinformatic analysis

Paired-end RNA-seq data were aligned to the human genome assembly (build hg38) using STAR (version 2.5a) with quantMode parameter set to 'TranscriptomeSAM'. Raw gene counts and Transcripts Per Million (TPM) values were calculated using RSEM (version 1.2.31) command rsem-calculate-expression. Differential expression analysis was performed using edgeR in R (v.3.5.3).

Pan-cancer gene expression profiles derived from The Cancer Genome Atlas (TCGA) database (https://portal.gdc.cancer.gov/) and normal samples from the Genotype-Tissue Expression (GTEx) project were used to build gene co-expression plots (https://gtexportal.org/home/index.html). Variance stabilizing transformation (VST) was applied to data before plotting, and correlation assessed using Spearman rank correlation method. Differential gene expression (DE) between treatments and control was assessed with DESeq2 v1.22.2, using default parameters.

Effects of TEPA or DC in the presence of IFNγ when compared with IFNγ alone, were calculated using limma empirical Bayes moderated t-statistics test (limma v3.38.3), and Benjamini-Hochberg correction applied. A corrected p-value $\leqslant 0.05$ was considered significant.

Gene Set Enrichment Analysis (GSEA) was performed using fgsea R package v1.8.0. Gene sets were derived from the Broad Institute's MSigDB collection (msigdbr v6.2.1), except for the STAT1 Targets gene set, which was built from the target list given in PMID 23645984. Immune deconvolution analysis using CIBERSORTx to impute cell fractions from the whole transcriptome expression tumor profile of the mice treated with TEPA, against the previously developed LM22 immune cells signature matrix(10, 11). Details on the Master Regulator analysis are provided in the supplementary materials.

Phospho-array

SH-SY5Y cells at 2.1 x10^6 were seeded in 75cm^2 flask and grown in DMEM media with 10% FBS for 24 hours. The day after the cells were treated with DC at 20μg/mL, TEPA at 2mM and Gefitinib at 10μM for 24 hours. Cells were scraped and lysed with ice-cold RIPA buffer containing proteinase and phosphatase inhibitors. Human Phospho-Kinase array kit (R&D System, cat # ARY003B) was used according to manufacturer's instructions.

Immunoprecipitation

SK-N-FI cells were seeded (~3.5 x 10^6/150cm2 flask) and grown in DMEM media with 10% FBS for 24h. The following day, cells were treated with MG132 (3μM) to inhibit the proteasome, 1h prior to treatment with TEPA (2mM) or Gefitinib (10μM) overnight. Cells were lysed in cold TNN buffer (50 mM Tris-HCl, pH 8.0; 150 mM NaCl; 5 mM EDTA; 0.5% NP-40) supplemented with protease and phosphatase inhibitors (Roche). After removing cell debris, lysates were pre-cleared with Protein A Dynabeads (Thermo Fisher) previously blocked in BSA. An aliquot of input lysates

were reserved before incubation with Rabbit IgG Isotype Control (Invitrogen, #10500C), anti-PD-L1 (CST, #13684) or anti-Ubiquitin (Abcam, ab7780) antibodies overnight on a rotating wheel at 4°C. Antibody-bound proteins were precipitated using blocked Protein A Dynabeads for 3h on a rotating wheel at 4°C. Washed beads were boiled in 1X Laemmli Sample Buffer (Bio-Rad) with 2.5% β-mercaptoethanol. Protein samples were separated using SDS-PAGE with anti-ubiquitin IP blots probed for PD-L1 and vice versa using the above antibodies. To prevent detection of heavy and light antibody chains, VeriBlot-HRP secondary antibody (Abcam, ab131366) was used. Proteins were visualized using the Bio-Rad Chemi-Doc Touch Imaging system.

Fluorescence confocal microscopy of STAT3

Phospho-STAT3 cellular localization was studied by fluorescence confocal microscopy. SH-SY5Y neuroblastoma cells were treated with IFNγ (2.5ng/ml, 2 h) or TEPA (2mM) and INFγ (2.5ng/ml) combination for 2hours. Cells were fixed in 4% formaldehyde and permeabilized with Triton X-100 0.4%. Cells were stained with Hoechst 33342 (1uM, 15 min) and phospho-STAT3 antibody (1:200; Cell signaling #9145) and Anti-rabbit IgG (H+L), F(ab')2 Fragment (1:2000 Alexa Fluor® 555 Conjugate; Cell signaling #4413). Imaging was performed with a confocal laser scanning microscope ZEISS LSM 880 with a Plan-Apochromat 63x/1.4 Oil DIC M27 objective (Zeiss). Phase images were captured using transmitted light (PMT). Airyscan z-stacks were captured with frame by frame sequential excitation using 405 nm and 561 nm lasers. Raw image data was deconvolved using the Airyscan processing algorithm in the Zen Black software package (SP3V2.1, Zeiss) and exported as orthogonal 2D TIFFS. Intensity profiles from representative single cells

were calculated for (A) IFNγ and (B) IFNγ + TEPA combination treatment, demonstrating channel localization and intensities along a defined trajectory. Intensity profiles calculated using ImageJ software.

Short term *in vivo* study

Treatments of Th-MYCN mice (n=4-6 per group, homozygous for MYCN oncogene) commenced when a palpable tumour (3.5 – 5 mm in diameter, around 6 weeks of age) was detectable as previously described by Weiss and colleagues (12). Mice were treated with the following copper-lowering agents: (i) DC at 300 µg/mL, single i.v. dose and (ii) TEPA at 400 mg/Kg/day oral-gavage, every 24h. DC-treated mice were collected at 24h and 48h, while TEPA-treated mice were collected at 24h, 48h, 72h and seven days. Serum was isolated and INFγ analyzed using the Mouse Cytokine Array (Abcam, #ab197465) according to the manufacturer's instructions.

Flow Cytometry study of tumor-infiltrating lymphocytes

Animals used in the biological studies were approved by the Animal Care and Ethics Committee at UNSW Australia (ACEC# 16/17B and ACEC#18/97B).

Treatments of Th-MYCN mice (n=4 per group) were commenced when a palpable tumor (3.5 – 5 mm in diameter) was detectable. Mice were treated to assess the short-term effect (72 hours) of the following copper-lowering agents: (i) DC at 300 µg/mL, single i.v. dose (ii) TEPA at 400 mg/Kg/day, three doses by oral gavage or (iii) PD-L1 antibody (BioXCell, InVivoPlus anti-mouse PD-L1, at 10 mg/Kg/day, single i.v. dose). 72 hours post-treatment, spleen (used for single control staining) and neuroblastoma tumors were excised and digested post-mortem using a cocktail of 1

mg/mL collagenase type IV (Sigma-Aldrich) and 0.02 mg/mL DNase (Sigma-Aldrich). Cells were then analyzed by flow cytometry.

In vivo survival studies

Treatments of *Th-MYCN*+/+ mice (7 mice/group) were started immediately after weaning (3 weeks of age). TEPA (400mg/Kg/day) treatment was administered daily for 5 consecutive days per week for a maximum of 3 weeks by oral gavage. Mice were humanely killed when the tumor size reached ~1cm^3 and blood, tumor and organs were collected.

Neuroblastoma xenograft mouse models

Animals used in the biological studies were approved by the Ethics Committee at UNSW Australia (ACEC# 18/97B) and animals were obtained from the Australian Bio Resources Facility (Moss Vale, NSW, Australia). Female BALB/c-Fox1nu/Ausb, 6-8 weeks old were injected subcutaneously into the right flank with 5x10^5 human SK-N-BE(2)-C cells suspended in 100µL PBS and growth factor–reduced Matrigel™ (BD Biosciences) at a 1:1 ratio. At day 7 post cell inoculation, when tumors reached a size of 100-200 mm^3, mice were randomized into treatment groups (4 mice per group) and treated daily by oral gavage for a total of 3 weeks with 200 mg/Kg/day, 400 mg/Kg/day or 800 mg/Kg/day of TEPA. Tumor size was measured using Vernier calipers and mice were euthanized once tumors reached 1,000 mm^3.

In vitro NK co-culture assay

NK cells, from healthy donor patients, were revived using NK media [X-vivo media (Lonza, cat #04380Q), 10% FBS, 1% Penicillin-Streptomycin-Glutamine, IL-2

(Miltenyi Biotech, cat #130-097-746 using 100U/mL)]. Cancer cells were seeded in tissue-culture treated 96-well plates at $1x10^4$ for neuroblastoma cell lines and $1.5x10^4$ for glioblastoma cell line. Then, the cells were incubated for 24h before addition of freshly diluted drug (DC, TEPA and IFNγ) or vehicle control. Media was then replaced with a ratio of 1:1 with NK cells (in NK media) and incubated for a maximum of 6h. Finally, NK cells were removed, and alive cancer cells were trypsinized and counted by Trypan blue exclusion method or analyzed by flow cytometry. For flow cytometry analysis, SH-SY5Y cells were seeded in tissue-culture treated 24-well plates at $1x10^5$ cells/well. 24h post DC or TEPA treatment, NK cells were added with a ratio of 1:1 (without removing drugs) and incubated for a maximum of 6h. Finally, stained cells were analyzed using the BD FACSCanto II Flow Cytometer and with FlowJo V10 software.

Statistical analysis

All in vitro experiments were repeated at least three times, and the means ± SEM were calculated. Associations among gene expressions were determined using two-sided Fisher's exact tests. The Mosaic plot was generated using R+ vcd package. Differences between two groups were determined with two-tailed Student's t tests (unpaired or paired where specified). Differences between three or more groups were determined using one-way ANOVA followed by Bonferroni's multiple comparison tests (for comparison to control means).

RESULTS

Positive correlation of CTR-1 and PD-L1 expression in cancer.

Copper transporter 1 (CTR-1) is a transmembrane pump responsible for Cu uptake in mammalian cells (13). Several reports have shown CTR-1 is highly expressed in different types of cancer that also feature elevated levels of Cu (5). In particular, we have previously shown that CTR-1 is highly expressed in NB tumors (6). To evaluate a potential association between the expression of CTR-1 and PD-L1, we performed immunohistochemistry (IHC) staining for both proteins in tissue-microarrays (TMAs), comprising biopsies from 90 NB patients and from 90 brain tumor patients, including GBM (Figs. 1A and 1B). 39% of NB's were negative for both CTR-1 and PD-L1, 42% were positive for CTR-1 and negative for PD-L1, while 19% of NB's were positive for both CTR-1 and PD-L1 (14). Whereas, 50% of brain tumor patients were negative for both CTR-1 and PD-L1, 41% were positive for CTR-1 and negative for PD-L1, and 9% were positive for both proteins (Figs. 1A, 1B, and 1C). We found a statistically significant association between CTR-1 and PD-L1 expression in both brain tumors (Phi=0.31 and p=0.006) and NB cases (Phi=0.38 and p<0.0001). In the overall cohort which includes 180 patients, 56% (100/180) showed CTR-1 positivity, 14% (25/180) were positive for both PD-L1 and CTR-1 and were positively associated (Phi=0.36; p<0.001).

Metallothioneins, such as MT1X (Metallothionein 1X), are proteins that are upregulated in conditions of metal excess. MT1X is used a surrogate measure of intracellular Cu, as its expression is proportional to intracellular Cu levels (15). For this reason, MT1X staining was performed on the same TMA as a positive control for the CTR1/copper signaling axis. In summary, 13% of NB's were negative for both MT1X and CTR-1, 4% were positive for MT1X and negative for CTR-1, while 67% of NB's were positive for both MT1X and CTR-1. Furthermore, 28% of brain tumor patients were negative for both MT1X and CTR-1, 11% were positive for MT1X and

negative for CTR-1, and 47% were positive for both proteins (Figs. 1A, 1B, and 1C). We found a statistically significant association between MT1X and CTR-1 expression in both brain tumors (Phi=0.47 and p<0.001) and NB cases (Phi=0.47 and p<0.001). In the overall cohort, 64% (116/180) showed MT1X positivity, 57% (102/180) were positive for both CTR-1 and MT1X and were positively associated (Phi=0.49; p<0.001).

A similar association was calculated between MT1X and PD-L1. 29% of NB's were negative for both MT1X and PD-L1, 52% were positive for MT1X and negative for PD-L1, while 19% of NB's were positive for both MT1X and PD-L1. Furthermore, 49% of brain tumor patients were negative for both MT1X and PD-L1, 43% were positive for MT1X and negative for PD-L1, and 8% were positive for both proteins (Figs. 1A, 1B, and 1C). We found a statistically significant association between MT1X and PD-L1 expression in both brain tumors (Phi=0.25 and p=0.018) and NB cases (Phi=0.31 and p=0.006). In the overall cohort, 13% (24/180) were positive for both PD-L1 and MT1X and were positively associated (Phi=0.29; p<0.001).

The mosaic plots summarize the distribution of CTR-1, PD-L1 and MT1X protein expression in the combined neuroblastoma and brain cancer cohorts (Fig. 1C). Notably, PD-L1 expression was only detected in patients with positive CTR-1 or MT1X expression.

To evaluate if this correlation was also present at the transcriptional level and in a wide range of cancers, we examined CTR-1 and PD-L1 mRNA expression in several cancers characterized by high Cu, including GBM, breast carcinoma, lung adenocarcinoma and stomach adenocarcinomas (16-19). Analysis of the Cancer Genome Atlas (TCGA) showed a significant positive correlation between CTR-1 and PD-L1 in all the tumor types analyzed (Figs. 2A and 2B). To further examine the

correlation between PD-L1 and intracellular copper we correlated the expression of PD-L1 with four copper-responsive genes (20): the metallothionein MT2A, the metal-responsive transcription factor MTF1, the nuclear factor erythroid 2-like2 NFE2L2 and the cellular prion protein PRNP. TCGA analysis showed a significant positive correlation between each of those four copper-responsive genes and PD-L1 in GBM and neuroendocrine tumors (Supplementary Fig. S1A). Subsequently, we wanted to determine whether the positive correlation of CTR-1 and PD-L1 is confined to tumor tissues. We therefore examined their mRNA expression levels in their corresponding normal tissues, using the Genotype-Tissue Expression (GTEx) database. Interestingly, we found no such association in normal adrenal gland (primary site for NB and neuroendocrine tumors) lung, colon, stomach, pancreas or spleen, while normal liver, breast, prostate and adipose tissues displayed a negative correlation between CTR-1 and PD-L1 expression (Fig. 2A; Supplementary Fig. S1B). As GBM can arise from several parts of the brain (21), we analyzed the expression of CTR-1 and PD-L1 in normal cerebellum, frontal cortex, anterior cingulate cortex, substantia nigra, hypothalamus, basal ganglia and cerebellar hemisphere, but again found no correlation in any region (Fig. 2B). Collectively, these findings suggest that the correlation between CTR-1 and PD-L1 is confined to tumor tissues.

Intracellular Cu levels influence PD-L1 expression in cancer cells

Given the critical role of CTR-1 in regulating copper levels, and the correlation between CTR-1 and PD-L1 in tumors, we hypothesized that intra-tumoral copper levels could affect PD-L1 expression in tumor cells. We tested this hypothesis in NB and GBM, which frequently display elevated Cu levels (6, 7). 1mM $CuCl_2$ was added to culture media of SH-SY5Y NB and U87MG GBM cells and PD-L1 protein

expression was monitored up to 8h (Figs 3A, 3B). Moreover, we showed a dose dependent effect of copper in increasing PD-L1 expression. Supplementing media of the cells with increasing doses of $CuCl_2$ (concentration range 20-200 µM) induced a proportional upregulation of PD-L1 (Supplementary Fig. S2A). These experiments clearly demonstrated that Cu supplementation induced PD-L1 upregulation *in vitro* in NB and GBM cell lines. Inductively coupled plasma mass spectrometry (ICP-MS) data confirmed that Cu supplementation increased intracellular Cu levels in both NB and GBM cell lines (Supplementary Fig. S2B). Interestingly, copper supplementation also upregulated PD-L1 mRNA levels in both cell lines (Fig. 3C). In this experiment IFNγ treatment was included as a positive control of PD-L1 stimulation (22). Again, MT1X levels were used as a surrogate measure of intracellular Cu.

As expected, MT1X mRNA was upregulated (>100-fold in SH-SY5Y, >10-fold in U87MG) when copper was added in the culture media, confirming elevated intracellular Cu uptake at 4h (Supplementary Fig. S2C), as registered in ICP-MS data (Supplementary Fig. S2B). Conversely, the use of Cu-chelating agent Tetraethylenepentamine (TEPA), which reduces the availability of copper in cells, caused a decrease in expression of MT1X (Supplementary Fig. S2D).

IFNγ is a pro-inflammatory cytokine produced by T cells and natural killer (NK) cells that induces PD-L1 upregulation in cancer cells enhancing immune-evasion (23). To determine whether Cu could stimulate signaling pathways activated by IFNγ and involved in PD-L1 driven immune evasion, RNA-sequencing was performed in SH-SY5Y NB cells incubated with $CuCl_2$. mRNA profiling clearly showed that Cu and IFNγ have similar effects on several pathways involved in PD-L1 expression and immune response to cancer. Gene set enrichment analysis (GSEA) revealed that 326 pathways are upregulated and 350 are downregulated by either Cu or IFNγ

stimulation (Supplementary Fig. S2E). Among these, we identified 4 signaling cascades known to be involved in tumor immunity: response to cytokines; regulation of cytokine production; IL6/JAK/STAT3 signaling (24) and TNF-a signaling via NF-kB which are key regulators of PD-L1 expression (23). Differential expression analysis (DE), comparing the changes in Cu-treated or IFNγ-treated cells against control cells, highlighted their strong overlap in regulating PD-L1 expression and other pathways driving immune-evasion (Figs 3D, 3E, 3F; Supplementary Figs S2E, S2F). Copper modulates oxidative phosphorylation in tumors and it activates EGFR phosphorylation (25) which in turn catalyzes STAT3 tyrosine phosphorylation (26, 27). This is consistent with our GSEA data showing that copper activates IL6/Jack/STAT3 signaling as well as IFNγ, leading to increased expression of PD-L1(Supplementary Fig S2F). Moreover, our GSEA data suggested that exposure to Cu induces inflammation via NF-kB mediated response pathway (Fig. 3F). NF–κB-mediated transcription is known to be a key regulator of the expression of numerous cytokines that influence the immunological properties of the tumor microenvironment. This includes increased PD-L1 expression in response to INFγ and other cytokines such as IL-12 and IL-1β (28). Overall, we can speculate that the high levels of copper in neuroblastoma cells can be important for transducing cytokine signals via NFκB, JAK/STAT and PI3K/Akt/mTOR/S6K, thus triggering PD-L1 upregulation. These findings prompted us to investigate whether reducing intracellular Cu could inhibit the induction of PD-L1 expression in response to IFNγ stimulation and thus potentially enhance anti-tumor immune response. Two approaches were adopted: (i) downregulation of Cu uptake using two independent siRNAs directed against CTR-1, and (ii) pharmacologically with either of two Cu-lowering drugs - Dextran-Catechin (DC) which inhibits Cu uptake (6) and TEPA (an analogue of the FDA approved Cu

chelator TETA (29)). Each siRNA caused a significant reduction of both CTR-1 protein expression (Fig. 3G) and intracellular Cu in SK-N-FI NB cells (Supplementary Fig. S2G). Consistent with our hypothesis a reduction in intracellular copper led to PD-L1 downregulation in cancer cells (Fig. 3G). This experiment was optimized to obtain a reduction in intracellular Cu (Supplementary Fig. S2G,). Cancer cells were next incubated either with 20μg/mL of DC or 2 mM TEPA for 24h (doses reducing copper but not affecting cell viability, Supplementary Fig. S2H-J), either in the presence or absence of IFNγ, to determine if Cu reduction could inhibit IFNγ-mediated PD-L1 induction. We demonstrated that both DC and TEPA downregulated PD-L1 protein in presence of IFNγ (Figs. 3H, 3I, and 3J, Supplementary Fig. S2I). In support of this finding, our RNA-seq data also showed that DC and TEPA significantly inhibited the IFNα/β/γ- transcriptional signature in SH-SY5Y NB cells (Fig. 3K, Supplementary Fig. S2K). Interestingly, only the Cu-chelating agent TEPA was able to decrease the immune response signature (including genes such as NFkB1A, KRAS, PIK3CD, CD38 and CD40) in NB cells (Supplementary Fig. 2L). This may be because TEPA binds Cu directly and its effect could be faster than DC, which indirectly reduces Cu uptake via depletion of CTR-1 expression (6).

Dextran-Catechin and TEPA downregulate PD-L1 expression by inhibiting EGFR and STAT phosphorylation signaling pathways.

PD-L1 expression is induced by the activation of oncogenic pathways, such as the epidermal growth factor receptor (EGFR) signaling pathway. EGFR stimulates three different signaling cascades: RAS/MEK/ERK, PI3K/mTOR/NF-kB and JAK/STAT, which in turn modulate anti-tumor immunity, in part by driving PD-L1 upregulation (30). As intracellular Cu is involved in phosphorylation of EGFR and the

RAS/MEK/ERK and PI3K/mTOR/NF-kB pathways in cancer cells (31), we investigated whether pharmacologically reducing intracellular Cu may affect the expression of kinases that regulate PD-L1 expression. A human phospho-kinase array was performed on SH-SY5Y NB cells incubated with DC, TEPA or the phospho-EGFR inhibitor Gefitinib (as positive control) (Fig. 4A) and found that copper-lowering drugs downregulated the phosphorylation of EGFR, AKT, TOR, ERK and STAT3 (Fig. 4B). Subsequently, we validated these results and confirmed that treatment with DC and TEPA inhibited EGFR phosphorylation, which in turn reduced PD-L1 expression in SH-SY5Y, SK-N-FI NB and U87MG GBM cells (Figs 4C and D; Supplementary Fig. S3A). As expected, cells exposed to Gefitinib (10 μM) also downregulated PD-L1 protein (Figs 4C and 4D). Conversely, increased intracellular Cu induced EGFR phosphorylation and PD-L1 upregulation (Supplementary Figs S3B and S3C). It is well known that AKT activation by EGFR is correlated with membrane PD-L1 expression (32). Moreover, recent investigations demonstrated that activation of AKT by EGFR suppresses GSK3β activity through Ser9 phosphorylation and this induced PD-L1 destabilization (33). To further prove that copper chelation downregulates EGFR signaling pathway we studied the effect of the copper chelators TEPA and DC on AKT and GSK3 β phosphorylation. Consistent with our hypothesis, data showed that TEPA and DC inhibited pAKTS473 and GSK3betaS9 phosphorylation in two different cell lines (Figure 4 E and 4F).
A recent study found that inhibition of EGFR activation and signaling destabilizes PD-L1, possibly via a balance between mono-multi versus poly-ubiquitination status (Fig. 4G) (34). To investigate whether Cu deprivation can increase the levels of ubiquitinated PD-L1 and PD-L1 degradation, we performed IP (immunoprecipitation) assay in SK-N-FI NB cells treated with TEPA and Gefitinib. We found that inhibition

of EGFR phosphorylation due to Cu deprivation by TEPA in SK-N-FI cells caused an accumulation of ubiquitinated PD-L1, potentially inducing degradation via the proteasome (Fig. 4H). To further prove that copper deprivation destabilized PD-L1, we examined the changes of PD-L1 protein half-life after treatment with DC. In these experiments we pre-treated cells with DC 20µg/ml for 12 h and then we added 200 µg/ml of cycloheximide (CHX) and incubated the cells for 2, 4, 8 and 12 h prior to preparing cell lysates for protein analysis. Cycloheximide exerts its effects by interfering with the translocation step in protein synthesis thus blocking eukaryotic translational elongation; however, it was well tolerated by cells up to 12h. Our results showed that under this experimental condition the PD-L1 half-life in SK-N-FI cells was 23.28 h, whereas when treated with DC PD-L1 half-life decreased to 13.76 h (Supplementary Fig. S3D). Moreover, to confirm that copper chelators affect the degradation rate of PD-L1, we performed a rescue experiment by using MG132, a potent and cell-permeable proteasome inhibitor. When cells were treated with MG132, both TEPA and Gefitinib were not able to reduce the PD-L1 protein level. This is because the degradation of PD-L1 which is induced by TEPA and Gefitinib was abrogated by the proteasome inhibitor MG132 (Supplementary Figs. 3E and 3F).

Our phospho-array data revealed for the first time that Cu lowering drugs reduced STAT3 phosphorylation (Figs. 4A and 4B). This result is particularly relevant, as phospho-STAT1 and phospho-STAT3 are involved in the activation of IFNγ-mediated PD-L1 expression (35). To validate this finding, SH-SY5Y NB cells were pre-incubated with DC and TEPA and then stimulated with IFNγ. We found that both agents caused a reduction of STAT3 phosphorylation, signifying reduced cell responsiveness to IFNγ (Fig. 5A). To further demonstrate the impact of copper

chelation in STAT signaling, we used immunofluorescence staining and confocal microscopy and observed decreased nuclear accumulation of phosphorylated STAT3 in cells treated with TEPA compared to the control cells (Fig. 5B). Moreover, to study the effect of copper chelation on STAT1 target genes we performed a bioinformatics methodology called Master Regulator analysis (Fig. 5C). This analysis is an algorithm used to identify transcription factors whose targets are enriched for a gene signature (e.g. a list of differentially expressed genes). Both these experiments clearly showed that in presence of copper chelation we have a less translocation of STAT3 in the nucleus and a downregulation of the transcription of the gene network target of STAT1. To better understand the effect of copper deprivation on the STAT signaling pathway, we interrogated a public data base of ChIP-Seq data for HeLa cells treated with IFNγ in order to obtain a comprehensive list of STATs target genes (36). When applied to our RNA-seq data, DC and TEPA were found to significantly reduce the expression of several STAT target genes (Figs. 5D, and 5E). Conversely, Cu and IFNγ induced upregulation of the same target gene set (Fig. 5E). Differential expression (DE) analysis, comparing the changes to untreated wild type cells is represented as a heatmap for SH-SY5Y treated with Cu, IFNγ, DC and TEPA with or without IFNγ (Figs. 5D and 5E). The heatmap clearly shows that both Cu and IFNγ have a similar stimulatory effect on the STAT target genes, whereas the copper lowering compounds DC and TEPA showed inhibitory effect.

Although we cannot exclude other indirect effects, our results show that Cu lowering drugs reduced PD-L1 expression potentially through two modes of action: firstly, at the transcriptional level by downregulating the JAK/STAT signaling pathway which in turn suppressed PD-L1 up-regulation in response to IFNγ stimulation; and secondly,

at a post-translational level by inhibiting EGFR signaling and promoting PD-L1 ubiquitination and degradation.

Cu-chelation enhances tumor-infiltration by immune cells and improves mouse survival by downregulating PD-L1 in NB tumors *in vivo.*

Our *in vitro* results prompted us to investigate the potential for Cu chelation to enhance the immune response to NB. For these *in vivo* experiments, we used the immune-competent transgenic NB mouse model, *Th-MYCN* (37). This model shares the major oncogenic driver with poor-outcome human NB and it recapitulates many of the features of the human disease. When tumors reached ~3 mm in diameter, mice were randomized to experimental groups that received either saline (control) group, TEPA or DC. TEPA was administered up to 7 days by oral gavage at a non-toxic dose typically used to control Cu accumulation *in vivo* (38). Alternatively, DC was given intravenously, and tumors collected 24h and 48h later. DC dosing and end points for the experiment were selected according to our previous PET imaging study that confirmed reduced intra-tumoral Cu (6).

IHC showed that TEPA and DC caused a significant time-dependent downregulation of PD-L1 expression (Figs. 6A and 6F). The PD-L1 downregulation was directly associated with decreased EGFR phosphorylation (Figs 6B and 6G) increased tumor infiltration by CD8+ Tumor Infiltrating Lymphocytes (TILs), CD244+ and CD335+ Natural Killer (NK) cells (Figs. 6C, 6D, 6E, 6H, 6I and 6J) in the same tumor samples. Western blot analysis further confirmed PD-L1 downregulation in lysates of the excised tumors, following treatment with either TEPA or DC (Supplementary Figs. S4A and S5A, respectively). The level of IFNγ was found elevated in the sera of mice treated with TEPA for one week, which is consistent with an increased anti-

cancer immune reaction (Supplementary Fig. S4B). Interestingly, this increased level of IFNγ was not able to induce PD-L1 upregulation in the tumors of mice treated with TEPA. This finding further supports the ability of copper chelating drugs to counteract the effect of IFNγ in inducing PD-L1 expression in the tumor.

DC-mediated CTR-1 downregulation in tumors was confirmed by IHC analysis (Supplementary Fig. S5B). TILs were also analyzed for their expression of CD4+ (T cells) and CD16+ (NK cells) following treatment with either TEPA or DC (Supplementary Figs. S4C, S4G, S5C, S5D and S5E, respectively). Flow cytometry analysis confirmed that TEPA and DC increased CD8+/CD4+ T and CD244+ NK cell infiltration, (Figs 7A, 7B and 7C). PD-L1 monoclonal antibody was injected in our NB mouse model as a positive control confirming the tumors were responsive to increased tumor immune cell infiltration in response to PD-L1/PD1 axis inhibition (Figs. 7A, 7B and 7C). Moreover, reducing copper levels in tumor cells with the copper lowering drugs, DC and TEPA, did not affect the expression of PD-1 in the CD4+ and CD8+ tumor infiltrating immune cells and of PD-L1 in the CD45+ (Figs. 7D, 7E and 7F). To further evaluate the effect of TEPA on composition of the tumor infiltrating cell population, we performed RNA-seq analysis from tumors derived from mice treated with TEPA for 72h and one week. We then performed an immune deconvolution analysis using CIBERSORTx to impute cell fractions from the whole transcriptome expression tumor profile of the mice treated with TEPA, against the previously developed LM22 immune cells signature matrix (10, 11). This experiment showed that TEPA has changed the composition of the tumor microenvironment by increasing the number of macrophages, lymphocytes CD4+, CD8+ and NK cells (Fig. 7G). This profound (about 3.5 times) increase in the CD8+ and CD4+ tumor infiltrating cells was followed by a mild increase of T regulatory cells (Treg), as

shown by the stain for CD25 and FOXP3 counts (Supplementary Figs. S4E and S4F). TEPA significantly increased the CD8:Treg ratio, indicating that this copper chelator induces an immune landscape consistent with an anti-tumor immune response.

The presence of CD8+ TILs is known to signify a favorable clinical outcome in a variety of tumors. Whereas NK effector function is known to be suppressed by PD-L1/PD-1 signaling, however a positive prognostic role for NK cells is far less clear (39). To examine the role of NK in our study, NB and GBM cells were pre-treated for 24h with DC or TEPA then co-cultured with primary peripheral blood NK cells. When we evaluated cancer cell viability by trypan blue exclusion and flow cytometry analysis, we found that exposure to either TEPA or DC resulted in enhanced NK-mediated death of various cancer cell lines (Supplementary Figs. S6A, S6B, S6C, S6D). As shown in Supplementary Fig. 6E, pre-treatment with DC or TEPA also reduced PD-L1 upregulation in response to IFNγ normally released by activated NK cells (40). Consistent with this finding, flow cytometry with 7-AAD staining showed increased NK-mediated cell death in SH-SY5Y cells pre-treated with Cu-lowering drugs, compared to the same NB cells co-cultured with NK cells in standard media (Supplementary Fig. S6F). To further confirm that increased susceptibility to NK cells was related to reduced Cu in cancer cells, we co-cultured NK cells with SK-N-FI NB cells, in which CTR-1 expression had been transiently knocked down. Despite showing normal viability and proliferation under control conditions, susceptibility to NK-mediated lysis was again confirmed (Supplementary Fig. S6G). Overall, our findings strongly indicate that reduced Cu levels may relieve NK exhaustion (41), by downregulating PD-L1 expression in their target cells.

Given the ability of TEPA to reduce PD-L1 expression and to increase TIL infiltration *in vivo*, we investigated whether Cu chelation would affect tumor growth and progression when used prophylactically in immune-competent NB-prone *Th-MYCN* transgenic mice. Mice (n=7 per group) commenced treatment immediately upon weaning at 21 days and were treated for three weeks with saline (control) or TEPA (400mg/Kg/day by oral gavage). As shown in Figs. 7H and 7I, TEPA significantly improved mouse survival compared to controls and reduced tumor growth. We were careful to avoid TEPA toxicity, which can typically arise with doses >550 mg/Kg/day (42). Indeed, no toxicity was evident during treatment, nor was weight loss observed (Supplementary Figs S7A), and no tissue abnormality was detected upon histopathological examination. To further investigate potential off-target effects of the treatment we examined the livers of neuroblastoma Th-MYCN mice treated with the copper chelator TEPA and did not observe any effect of the drug on CTR-1 and PD-L1 expression in this organ (Supplementary Fig. 7B). We chose liver, because it is the organ which is the physiological storage of copper in the body and can be the most affected by the use of copper lowering drugs. Moreover, analysis of publicly available genetic data of normal liver showed no correlation between the expression of CTR-1 and PD-L1 (Supplementary Fig. S1).

To obtain further proof of the important role of the immune cells in the anticancer activity of TEPA, we demonstrated that the same concentration which reduced tumor growth and increased survival in the transgenic neuroblastoma Th-MYCN mice (Fig. 7H), did not affect tumor growth when administered to an immunocompromised NB mouse model (Supplementary Fig. S7C).

Together, our results support a key role of Cu homeostasis in cancer immune evasion.

DISCUSSION

The PD-L1/PD-1 axis is a major therapeutic target in cancer immune modulation therapy, and antibody-mediated blockade therapies have demonstrated good clinical results, mainly in adult melanoma and lung cancer. Unfortunately, this approach has not been as successful as expected for other solid tumors. Moreover, immune checkpoint inhibitor therapy is very costly and is also associated with several side effects, including rashes, diarrhea, colitis, inflammatory arthritis and many others frequently leading to treatment interruption (43, 44). Although we have seen rapid clinical translation of PD-L1/PD-1 inhibitors, there is still a dearth of knowledge about the mechanisms regulating PD-L1 expression in cancer cells, which limits our ability to design and develop new approaches to overcome resistance and reduce side effects.

Several mechanisms have been described to lead to aberrant PD-L1 activation, such as genomic alterations, constitutive activation of oncogenic signaling such as EGFR, mTOR, PI3K, AKT and PTEN deletion (45-48), extrinsic factors such as pro-inflammatory cytokines IFNγ, TGF1β1, TNFα and IL-17 (49-51). Since PD-L1 expression in normal tissue regulates self-tolerance, it is also important to understand what makes its expression aberrant specifically in tumors; this will in turn allow us to develop therapies targeting PD-L1 in tumors potentially without affecting the normal mechanism of self-tolerance. Here, we identify a strong positive correlation between CTR-1 and PD-L1 present predominantly in malignant tissues, by comparison with normal matched tissues. This is consistent with the higher copper levels present in NB and GBM tumors, compared to normal tissues, and with our discovery that elevated copper induces PD-L1 gene transcription and

protein stabilization. Conversely, copper chelating agents decreased PD-L1 expression via inhibition of the response of the cancer cells to pro-inflammatory cytokines IFNγ, TNF-α and IFN-α/β. Moreover, although we cannot exclude other potential indirect effects of copper chelators, we demonstrated that copper depletion in cancer cells downregulates STAT3, EGFR, AKT and GSK3β phosphorylation, which inhibits the transcription of PD-L1 and regulates PD-L1 ubiquitination and stabilization/degradation, respectively.

Our results are consistent with recent work showing that the copper ionophore Disulfiram can induce stabilization of PD-L1 by overloading cancer cells with copper (52). Although several studies and clinical trials have proved that copper is important in cancer progression and that copper chelators are effective in inhibiting tumor growth and angiogenesis, we are the first to show that chelation therapy enhances anti-tumor immune responses and could be repurposed for immune checkpoint inhibition. We have provided crucial evidence of using the copper chelator TEPA to increase tumor infiltrating immune cells and improve the survival in a neuroblastoma immunocompetent mouse model. Although some of the reduction in tumor size may be a consequence of decrease in angiogenesis or cell proliferation, this is an impressive result considering the aggressiveness of this model and that we used TEPA as a single agent. Moreover, results showing that TEPA did not affect tumor growth in an immunocompromised NB xenograft model provides further evidence that the anti-tumor effect of TEPA and improved survival in the immunocompetent mouse model may be caused by the stimulation of an anti-cancer immune response. The increased number of TILs observed in response to copper chelation could be a consequence of the PD-L1 blockade, which stimulates

new T cells clones to enter the tumor, as recently shown by Yost and colleagues (53).

Since there are many types of cancer whose progression has been demonstrated to be copper-dependent this new immune therapeutic approach has strong potential to be advanced to the clinic. Repurposing clinically available copper chelating drugs as immune checkpoint inhibitors is an appealing and attractive strategy, considering that they are not cytotoxic, have minimal effects on immune cells and that they seem to be more active in reducing PD-L1 expression specifically in tumors. The high correlation between copper levels and PD-L1 expression specifically in transformed tissues, led us to hypothesize that this novel therapeutic approach may reduce the immune-related adverse events which are a major limitation of the current anti-PD-L1 blockade therapy. Moreover, the low-cost of chelation therapy makes this novel therapeutic approach suitable for future combination with other immunotherapies, including the highly expensive and laborious CAR T cell therapy.

In conclusion, this study describes a novel causal link between intra-tumoral copper and the regulation of PD-L1, paving the way for clinical trials to evaluate copper chelators as immune checkpoint inhibitors.

Acknowledgements:

The authors acknowledge Children's Cancer Institute, which is affiliated with the Sydney Children's Hospital and School of Women's & Children's Health, UNSW Sydney. The authors also thank the Sydney Children's Tumour Bank Network (in particular A/Prof D. Catchpoole and Ms A. Yuksel from the Children's Hospital at Westmead Tumour Bank) for providing the TMA slides and related clinical information for this study.

Author's contribution:

Conception and design: F.V., E.V., F.S., F.M.G., P. A.B., J.A.T., M.K., O.V.

Development of methodology: F.V., L.L., E.V., K.K., F.S., F.M.G., D.M., S.S., J.M., A. A.C., G.C., P.A.B., O.V.

Acquisition of data (provided animals, acquired and managed patients, provided facilities, etc.): F.V., E.V., K.K., F.S., S.S., J.M., G.C., C.M., O.V.

Analysis and interpretation of data (e.g., statistical analysis, biostatistics, computational analysis): F.V., E.V., F.S., F.M.G., D.M., S.S., J.M., C.M., P. A.B., O.V.

Writing, review, and/or revision of the manuscript: F.V., E.V., F.S., F.M.G., P.A.B., M.H., J.A.T., M.K., O.V.

Administrative, technical, or material support (i.e., reporting or organizing data, constructing databases): F.V., E.V., F.S., J.R., F.M.G., D.M., C.M., P.A.B., O.V.

Study supervision: P. A.B., M.H., J.A.T., M.K., O.V.

Other (execution of experiments): F.V., L.L., E.V., K.K., F.S., F.M.G., D.M., S.S., J.M., O.V.

REFERENCES

1. Iwai Y, Ishida M, Tanaka Y, Okazaki T, Honjo T, and Minato N. Involvement of PD-L1 on tumor cells in the escape from host immune system and tumor immunotherapy by PD-L1 blockade. *Proc Natl Acad Sci U S A.* 2002;99(19):12293-7.
2. Zhang T, Xie J, Arai S, Wang L, Shi X, Shi N, et al. The efficacy and safety of anti-PD-1/PD-L1 antibodies for treatment of advanced or refractory cancers: a meta-analysis. *Oncotarget.* 2016;7(45):73068-79.
3. Chen L, Diao L, Yang Y, Yi X, Rodriguez BL, Li Y, et al. CD38-Mediated Immunosuppression as a Mechanism of Tumor Cell Escape from PD-1/PD-L1 Blockade. *Cancer Discov.* 2018;8(9):1156-75.
4. Postow MA, Sidlow R, and Hellmann MD. Immune-Related Adverse Events Associated with Immune Checkpoint Blockade. *N Engl J Med.* 2018;378(2):158-68.

5. Denoyer D, Masaldan S, La Fontaine S, and Cater MA. Targeting copper in cancer therapy: 'Copper That Cancer'. *Metallomics.* 2015;7(11):1459-76.
6. Parmar A, Pascali G, Voli F, Lerra L, Yee E, Ahmed-Cox A, et al. In vivo [(64)Cu]CuCl2 PET imaging reveals activity of Dextran-Catechin on tumor copper homeostasis. *Theranostics.* 2018;8(20):5645-59.
7. Lun XQ, Wells JC, Grinshtein N, King JC, Hao XG, Dang NH, et al. Disulfiram when Combined with Copper Enhances the Therapeutic Effects of Temozolomide for the Treatment of Glioblastoma. *Clinical Cancer Research.* 2016;22(15):3860-75.
8. Jones DG. Effects of Dietary Copper Depletion on Acute and Delayed Inflammatory Responses in Mice. *Research in Veterinary Science.* 1984;37(2):205-10.
9. Vittorio O, Brandl M, Cirillo G, Kimpton K, Hinde E, Gaus K, et al. Dextran-Catechin: An anticancer chemically-modified natural compound targeting copper that attenuates neuroblastoma growth. *Oncotarget.* 2016;7(30):47479-93.
10. Newman AM, Liu CL, Green MR, Gentles AJ, Feng W, Xu Y, et al. Robust enumeration of cell subsets from tissue expression profiles. *Nat Methods.* 2015;12(5):453-7.
11. Newman AM, Steen CB, Liu CL, Gentles AJ, Chaudhuri AA, Scherer F, et al. Determining cell type abundance and expression from bulk tissues with digital cytometry. *Nat Biotechnol.* 2019;37(7):773-82.
12. Weiss WA, Aldape K, Mohapatra G, Feuerstein BG, and Bishop JM. Targeted expression of MYCN causes neuroblastoma in transgenic mice. *The EMBO journal.* 1997;16(11):2985-95.
13. Stefaniak E, Plonka D, Drew SC, Bossak-Ahmad K, Haas KL, Pushie MJ, et al. The N-terminal 14-mer model peptide of human Ctr1 can collect Cu(ii) from albumin. Implications for copper uptake by Ctr1. *Metallomics.* 2018;10(12):1723-7.
14. Saletta F, Vilain RE, Gupta AK, Nagabushan S, Yuksel A, Catchpoole D, et al. Programmed Death-Ligand 1 Expression in a Large Cohort of Pediatric Patients With Solid Tumor and Association With Clinicopathologic Features in Neuroblastoma. *Jco Precision Oncology.* 2017;1.
15. Muller P, van Bakel H, van de Sluis B, Holstege F, Wijmenga C, and Klomp LW. Gene expression profiling of liver cells after copper overload in vivo and in vitro reveals new copper-regulated genes. *J Biol Inorg Chem.* 2007;12(4):495-507.
16. Diez M, Arroyo M, Cerdan FJ, Munoz M, Martin MA, and Balibrea JL. Serum and tissue trace metal levels in lung cancer. *Oncology.* 1989;46(4):230-4.
17. Gupta SK, Shukla VK, Vaidya MP, Roy SK, and Gupta S. Serum and tissue trace elements in colorectal cancer. *J Surg Oncol.* 1993;52(3):172-5.
18. Huang YL, Sheu JY, and Lin TH. Association between oxidative stress and changes of trace elements in patients with breast cancer. *Clin Biochem.* 1999;32(2):131-6.
19. Yaman M, Kaya G, and Yekeler H. Distribution of trace metal concentrations in paired cancerous and non-cancerous human stomach tissues. *World J Gastroenterol.* 2007;13(4):612-8.
20. Song MO, and Freedman JH. Expression of copper-responsive genes in HepG2 cells. *Molecular and cellular biochemistry.* 2005;279(1-2):141-7.
21. Larjavaara S, Mantyla R, Salminen T, Haapasalo H, Raitanen J, Jaaskelainen J, et al. Incidence of gliomas by anatomic location. *Neuro Oncol.* 2007;9(3):319-25.
22. Mandai M, Hamanishi J, Abiko K, Matsumura N, Baba T, and Konishi I. Dual Faces of IFNgamma in Cancer Progression: A Role of PD-L1 Induction in the Determination of Pro- and Antitumor Immunity. *Clin Cancer Res.* 2016;22(10):2329-34.
23. Cha JH, Chan LC, Li CW, Hsu JL, and Hung MC. Mechanisms Controlling PD-L1 Expression in Cancer. *Mol Cell.* 2019.
24. Johnson DE, O'Keefe RA, and Grandis JR. Targeting the IL-6/JAK/STAT3 signalling axis in cancer. *Nat Rev Clin Oncol.* 2018;15(4):234-48.
25. Ishida S, Andreux P, Poitry-Yamate C, Auwerx J, and Hanahan D. Bioavailable copper modulates oxidative phosphorylation and growth of tumors. *Proceedings of the National Academy of Sciences.* 2013;110(48):19507-12.
26. Bhat AA, Lu H, Soutto M, Capobianco A, Rai P, Zaika A, et al. Exposure of Barrett's and esophageal adenocarcinoma cells to bile acids activates EGFR–STAT3 signaling axis via induction of APE1. *Oncogene.* 2018;37(46):6011-24.
27. Hsu P-Y, Yen H-H, Yang T-H, and Su C-C. Tetrathiomolybdate, a copper chelator inhibited imiquimod-induced skin inflammation in mice. *Journal of dermatological science.* 2018;92(1):30-7.
28. Richmond A, and Yang J. The role of NF-kB in modulating antitumor immunity. *OncoImmunology.* 2016;5(1):e1005522.
29. Dahlman T, Hartvig P, Lofholm M, Nordlinder H, Loof L, and Westermark K. Long-term treatment of Wilson's disease with triethylene tetramine dihydrochloride (trientine). *QJM.* 1995;88(9):609-16.

30. Zhang N, Zeng Y, Du W, Zhu J, Shen D, Liu Z, et al. The EGFR pathway is involved in the regulation of PD-L1 expression via the IL-6/JAK/STAT3 signaling pathway in EGFR-mutated non-small cell lung cancer. *Int J Oncol.* 2016;49(4):1360-8.
31. Brady DC, Crowe MS, Turski ML, Hobbs GA, Yao X, Chaikuad A, et al. Copper is required for oncogenic BRAF signalling and tumorigenesis. *Nature.* 2014;509(7501):492-6.
32. Akbay EA, Koyama S, Carretero J, Altabef A, Tchaicha JH, Christensen CL, et al. Activation of the PD-1 pathway contributes to immune escape in EGFR-driven lung tumors. *Cancer Discov.* 2013;3(12):1355-63.
33. Li C-W, Lim S-O, Xia W, Lee H-H, Chan L-C, Kuo C-W, et al. Glycosylation and stabilization of programmed death ligand-1 suppresses T-cell activity. *Nature Communications.* 2016;7(1):12632.
34. Horita H, Law A, Hong S, and Middleton K. Identifying Regulatory Posttranslational Modifications of PD-L1: A Focus on Monoubiquitinaton. *Neoplasia.* 2017;19(4):346-53.
35. Qing Y, and Stark GR. Alternative activation of STAT1 and STAT3 in response to interferon-gamma. *J Biol Chem.* 2004;279(40):41679-85.
36. Satoh J, and Tabunoki H. A Comprehensive Profile of ChIP-Seq-Based STAT1 Target Genes Suggests the Complexity of STAT1-Mediated Gene Regulatory Mechanisms. *Gene Regul Syst Bio.* 2013;7:41-56.
37. Weiss WA, Aldape K, Mohapatra G, Feuerstein BG, and Bishop JM. Targeted expression of MYCN causes neuroblastoma in transgenic mice. *EMBO J.* 1997;16(11):2985-95.
38. Greenman DL, Morrissey RL, Blakemore W, Crowell J, Siitonen P, Felton P, et al. Subchronic toxicity of triethylenetetramine dihydrochloride in B6C3F1 mice and F344 rats. *Fundam Appl Toxicol.* 1996;29(2):185-93.
39. Concha-Benavente F, Kansy B, Moskovitz J, Moy J, Chandran U, and Ferris RL. PD-L1 Mediates Dysfunction in Activated PD-1(+) NK Cells in Head and Neck Cancer Patients. *Cancer Immunol Res.* 2018;6(12):1548-60.
40. Wang R, Jaw JJ, Stutzman NC, Zou Z, and Sun PD. Natural killer cell-produced IFN-gamma and TNF-alpha induce target cell cytolysis through up-regulation of ICAM-1. *J Leukoc Biol.* 2012;91(2):299-309.
41. Bi J, and Tian Z. NK Cell Exhaustion. *Front Immunol.* 2017;8:760.
42. Hernandez O. TETRAETHYLENEPENTAMINE CAS N°: 112-57-2. 2002.
43. Myers G. Immune-related adverse events of immune checkpoint inhibitors: a brief review. *Curr Oncol.* 2018;25(5):342-7.
44. Abdel-Wahab N, Alshawa A, and Suarez-Almazor ME. Adverse Events in Cancer Immunotherapy. *Adv Exp Med Biol.* 2017;995:155-74.
45. Lastwika KJ, Wilson W, 3rd, Li QK, Norris J, Xu H, Ghazarian SR, et al. Control of PD-L1 Expression by Oncogenic Activation of the AKT-mTOR Pathway in Non-Small Cell Lung Cancer. *Cancer Res.* 2016;76(2):227-38.
46. Song M, Chen D, Lu B, Wang C, Zhang J, Huang L, et al. PTEN loss increases PD-L1 protein expression and affects the correlation between PD-L1 expression and clinical parameters in colorectal cancer. *PLoS One.* 2013;8(6):e65821.
47. Jiang X, Zhou J, Giobbie-Hurder A, Wargo J, and Hodi FS. The activation of MAPK in melanoma cells resistant to BRAF inhibition promotes PD-L1 expression that is reversible by MEK and PI3K inhibition. *Clin Cancer Res.* 2013;19(3):598-609.
48. Chen N, Fang W, Zhan J, Hong S, Tang Y, Kang S, et al. Upregulation of PD-L1 by EGFR Activation Mediates the Immune Escape in EGFR-Driven NSCLC: Implication for Optional Immune Targeted Therapy for NSCLC Patients with EGFR Mutation. *J Thorac Oncol.* 2015;10(6):910-23.
49. Wang X, Yang L, Huang F, Zhang Q, Liu S, Ma L, et al. Inflammatory cytokines IL-17 and TNF-alpha up-regulate PD-L1 expression in human prostate and colon cancer cells. *Immunol Lett.* 2017;184:7-14.
50. Alsuliman A, Colak D, Al-Harazi O, Fitwi H, Tulbah A, Al-Tweigeri T, et al. Bidirectional crosstalk between PD-L1 expression and epithelial to mesenchymal transition: significance in claudin-low breast cancer cells. *Mol Cancer.* 2015;14:149.
51. Garcia-Diaz A, Shin DS, Moreno BH, Saco J, Escuin-Ordinas H, Rodriguez GA, et al. Interferon Receptor Signaling Pathways Regulating PD-L1 and PD-L2 Expression. *Cell Rep.* 2017;19(6):1189-201.
52. Zhou B, Guo L, Zhang B, Liu S, Zhang K, Yan J, et al. Disulfiram combined with copper induces immunosuppression via PD-L1 stabilization in hepatocellular carcinoma. *American journal of cancer research.* 2019;9(11):2442-55.
53. Yost KE, Satpathy AT, Wells DK, Qi Y, Wang C, Kageyama R, et al. Clonal replacement of tumor-specific T cells following PD-1 blockade. *Cancer Discov.* 2019;25(8):1251-9.

Figure legends:

Figure 1. Positive correlation at the protein level between CTR-1, PD-L1 and MT1X in neuroblastoma and brain tumor patients. Representative images of CTR-1, PD-L1 and MT1X negative (Neg) and positive staining (Pos) of **A,** neuroblastoma (NB) and **B,** brain tumor patients. Black bars represent 200μm. **C**, Mosaic Plot utilized to graphically describe the protein expression distribution of CTR-1, PD-L1 and MT1X in the whole tumor cohort. The colors indicate the level of the Pearson residual for each combination and represent which cells are contributing to the significance of the chi-squared test result. Specifically, “blue” indicates that there are more observations in that cell than would be expected under the null model (independence) while “red” means there are fewer observations than would have been expected. Bivariate relationships between CTR-1-PD-L1- and MT1X-positive were analyzed using cross tabulation and the association between expressions was determined using Pearson correlation coefficient (Phi coefficient), while significance was tested using Fisher’s exact test.

Figure 2. Positive correlation at the mRNA level between the expression of CTR-1 and PD-L1 in cancer. **A and B,** Co-expression plots of VST-normalized gene expression profiles derived from TCGA datasets (for malignant tissues) and from GTEX datasets (for normal tissues), including sub-areas of the human brain.

Sample size is indicated, with Spearman Correlation Coefficient (SCC) and correlation p-value. Background color indicates significant correlation ($p \leqslant 0.01$): if red, positive correlation, if blue, negative correlation. A regression line is shown in the graph. VST (Variance Stabilizing Transformation, Anders & Huber 2010).

Figure 3. Intracellular copper levels influence PD-L1 expression in cancer cells. PD-L1 protein expression determined by western blot after copper addition (1mM up to 8h) in **A**, SH-SY5Y cells and in **B**, U87 cells (1mM up to 4h). Densitometry analysis of PD-L1 protein relative to actin are reported as average of at least 3 independent western blots PD-L1. **C**, mRNA levels in SH-SY5Y and U87MG cells treated with copper (CuCl2, 1 mM, 4h) or with IFNγ (2.5 ng/mL for SH-SH5Y and 7.5 ng/mL for U87MG cells, 24h); Data represents mean of at least three experiments, deviation calculated as SEM. Ordinary one-way ANOVA followed by Bonferroni's multiple comparison test was used for statistical significance (* $p<0.05$, ** $p<0.01$, *** $p<0.001$, **** $p<0.0001$). **D, E, F**, Gene Set Enrichment Analysis (GSEA) enrichment plot of the indicated pathways from the Broad Institute's MSigDB in Copper- and IFNγ- treated SH-SY5Y cells. The heatmap shows the clustered genes in the leading edge of the Copper subset. Color intensity is representative of the DESeq2 DE statistic values (scaled). **G**, Western blot analysis of SK-N-FI cells transiently transfected with two different siRNAs for CTR-1. Treatment (24h) with Dextran-Catechin (DC) or TEPA, in combination with IFNγ, decreased PD-L1 expression in **H**, SH-SY5Y, **I**, SK-N-BE(2)-C and **J**, SK-N-FI cells. **K**, Gene Set Enrichment Analysis (GSEA) enrichment plot of the indicated pathway from the Broad Institute's MSigDB in SH-SY5Y cells treated with TEPA + IFNγ or DC + IFNγ. The heatmap shows the clustered genes in the leading edge of the TEPA + IFNγ

subset. Color intensity is representative of VST-normalized gene expression. Biological replicates per treatment condition are shown.

Figure 4. Dextran-Catechin and TEPA downregulate PD-L1 expression by decreasing EGFR and STAT3 signaling pathways. A and B, Representative image of human phospho-kinase array performed in SH-SY5Y treated for 24h with DC, TEPA or Gefitinib (positive control). Normalized expression relative to control is shown for phosphorylated EGFR, AKT, TOR, ERK, JNK, and STAT3. Data represents the mean of at least two separate experiments. **C and D**, Expression of phospho-EGFR (Y1068) and PD-L1 in SH-SY5Y and U87MG cells, 24h after treatment with DC, TEPA or gefitinib; densitometry analysis of phospho-EGFR and PD-L1 proteins relative to actin are reported as average of at least 3 independent western blots. **E and F**, Expression of AKT and GSK3β phosphorylation in SH-SY5Y and SK-N-FI cells, 24h after treatment with DC, TEPA; densitometry analysis of phospho-AKT and phospho-GSK3β proteins relative to AKT total and GSK3β total are reported as average of at least 3 independent western blots. **G**, Schematic representation of PD-L1 post-translational modifications related to ubiquitination status. Adapted from Horita et al., Neoplasia, 2017. **H**, Expression levels of ubiquitinated PD-L1 in SK-N-FI cells pre-treated with proteasome inhibitor MG132 for 1h, followed by IFNγ addition (C = Control; T = TEPA; G = Gefitinib) for 24h. Top panel represents anti-ubiquitin IP blot probed for PD-L1, while the middle panel shows anti-PD-L1 IP blot probed for ubiquitin. The bottom blot shows the input of the middle panel at lower exposure.

Figure 5. Dextran-Catechin and TEPA downregulate PD-L1 expression by decreasing STAT signaling pathway. A, Expression of phospho-STAT1 (Y701), phospho-STAT3 (Y705) and total levels of STAT1/3 in SH-SY5Y cells pre-treated with DC or TEPA for 2h and then stimulated with IFNγ for additional 2h, without removing previous drugs; densitometry analysis of phospho-STAT1 (Y701) and phospho-STAT3 (Y705) relative to STAT1 and STAT3 total are reported as average of at least 3 independent western blots. **B**, Phospho-STAT3 cellular localization examined by fluorescence confocal microscopy: intensity profiles from representative single cells were calculated for IFNγ and IFNγ + TEPA combination treatment, demonstrating channel localization and intensities along a defined trajectory. Intensity profiles calculated using ImageJ software. **C,** MRA results obtained through the mra plot function of the R CRAN package corto. STAT1 network was found to be significantly downregulated in TEPA treated cells. Genes in each network are shown in a barcode-like diagram from most downregulated (left) to most upregulated (right). The 12 top differentially influenced STAT1 putative targets are shown to the right. Each target is shown in red if it is differentially upregulated, or blue if downregulated. A pointed arrow indicates that the target is predicted to be activated by STAT1, while a blunt arrow indicates a predicted repression. **D,** Gene Set Enrichment Analysis (GSEA) enrichment plot of STAT1 Targets pathway in SH-SY5Y cells treated with IFNγ + TEPA, IFNγ+ DC or TEPA, DC, IFNγ and copper alone. **E**, STAT1 target genes set derived from the previously published STAT1 ChIP-Seq based target list [PMID 23645984]. Heatmap showing the clustered genes in the leading-edge analysis of the Copper subset. Color intensity is representative of the DESeq2 DE statistic values (scaled). Expression data of samples IFNγ + DC and IFNγ + TEPA is referred to the analysis vs. IFNγ treatment alone, whereas samples Copper, DC and

TEPA is referred to the analysis vs. untreated cells as described in materials and methods.

Figure 6. Copper chelation therapy enhances the number of tumor-infiltrating immune cells in *Th-MYCN* transgenic mouse NB tumors. Immunohistochemistry staining in NB tumor slices for **A**, PD-L1, **B**, phospho-EGFR, **C**, CD8, **D**, CD244 and **E**, CD335 dissected from *Th-MYCN* mice treated with TEPA (400mg/Kg/day) for 72h or one week. Immunohistochemistry staining in NB tumor slices for **F**, PD-L1, **G**, phospho-EGFR, **H**, CD8, **I**, CD244 and **J,** CD335 dissected from *Th-MYCN* mice treated with DC (300 μg/mL) for 24h or 48h. Images are representative of 4 mice for saline control group and 6 mice for each treatment time-point. Black bars represent 60μm. The bar graphs show PD-L1 H-score or CD8/CD244/CD335 cell density (* $p<0.05$; ** $p<0.01$; *** $p<0.001$). Cell density is expressed as number of cells/field, with a field size of $0.1mm^2$.

Figure 7. Copper chelation therapy enhances *Th-MYCN* transgenic mouse survival by downregulating PD-L1 expression *in vivo*. A, B, C, Flow cytometry analysis for CD8, CD4 and CD244 staining (positive cells per mg of tumor) from *Th-MYCN* transgenic mice (n=5) treated with DC (300 μg/mL), TEPA (400mg/kg/day) or murine anti PD-L1 antibody (10mg/kg/day) for 72h. **D, E**, Expression of PD-1 in CD4 and CD8 positive cells and **F**, PD-L1 in CD45+ infiltrating cells.
Data were obtained from tumor-bearing mice (n=5) treated with saline control (red dots), with DC (blue square), TEPA (green triangles) for 72h. Cell density is expressed as a ratio between the number of positive cells and tumor weight. Mean

fluorescence intensity (MFI) for PD-L1 in CD45 positive cells and for PD-1 in CD4 and CD8 positive cells. Unpaired two-tailed t-test was used for statistical significance (* $p<0.05$, ** $p<0.01$). **G**, Immune deconvolution analysis using CIBERSORTx to impute cell fractions from the whole transcriptome expression profile against the previously developed LM22 immune cells signature matrix. **H,** Survival curve of *Th-MYCN* transgenic mice (n=7 per group) treated with saline control (blue line), or TEPA (red line). Log-rank (Mantel-Cox) test was used for statistical significance ($p=0.006$). **I,** Tumor growth of mice treated with saline control (blue line), or TEPA (red line).

Figure 1

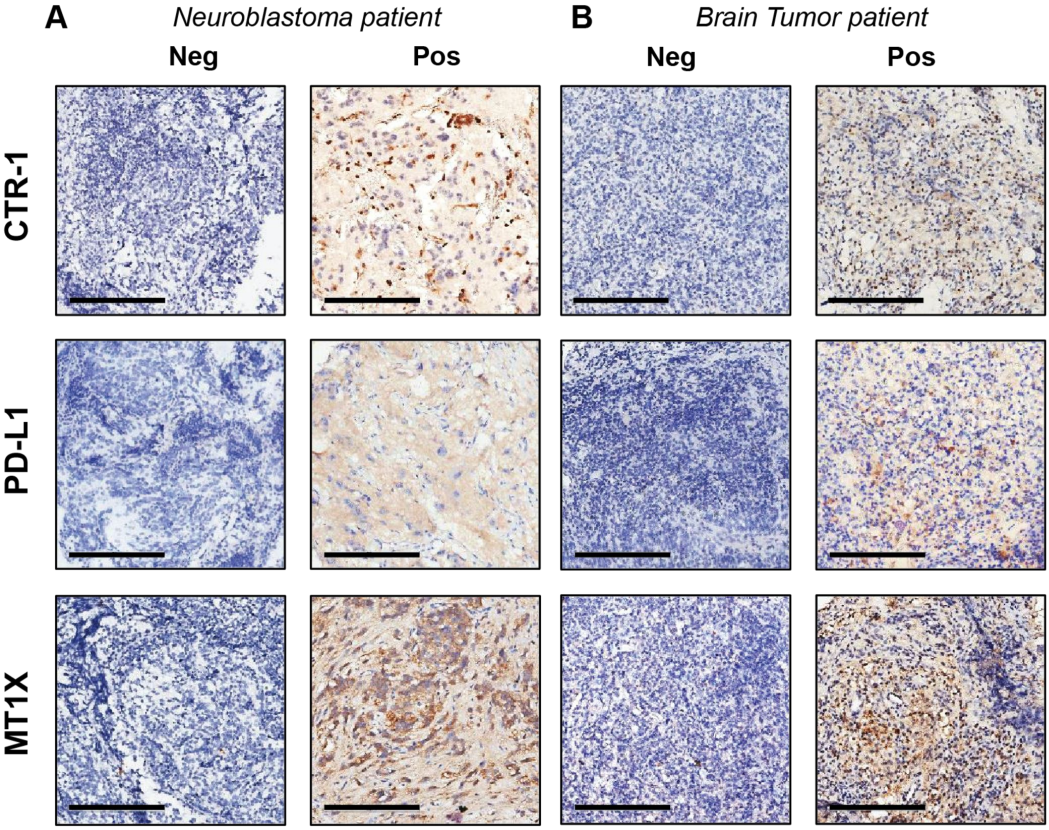
A
Neuroblastoma patient
B
Brain Tumor patient
Neg
Pos
Neg
Pos
CTR-1
PD-L1
MT1X

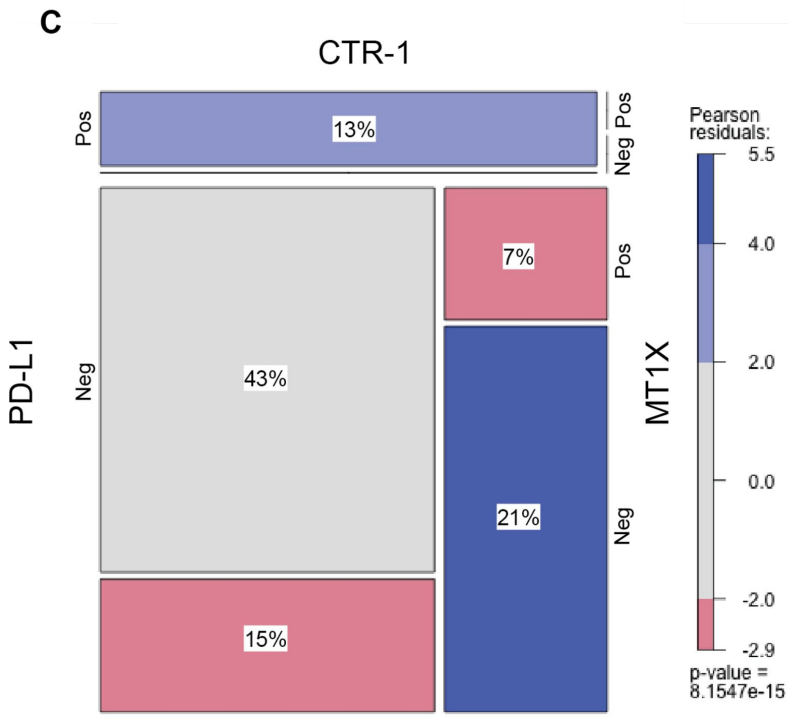
C
CTR-1
Pos
13%
Neg
Pos
7%
Pos
PD-L1
Neg
43%
21%
Neg
MT1X
15%
Pearson residuals:
5.5
4.0
2.0
0.0
-2.0
-2.9
p-value =
8.1547e-15

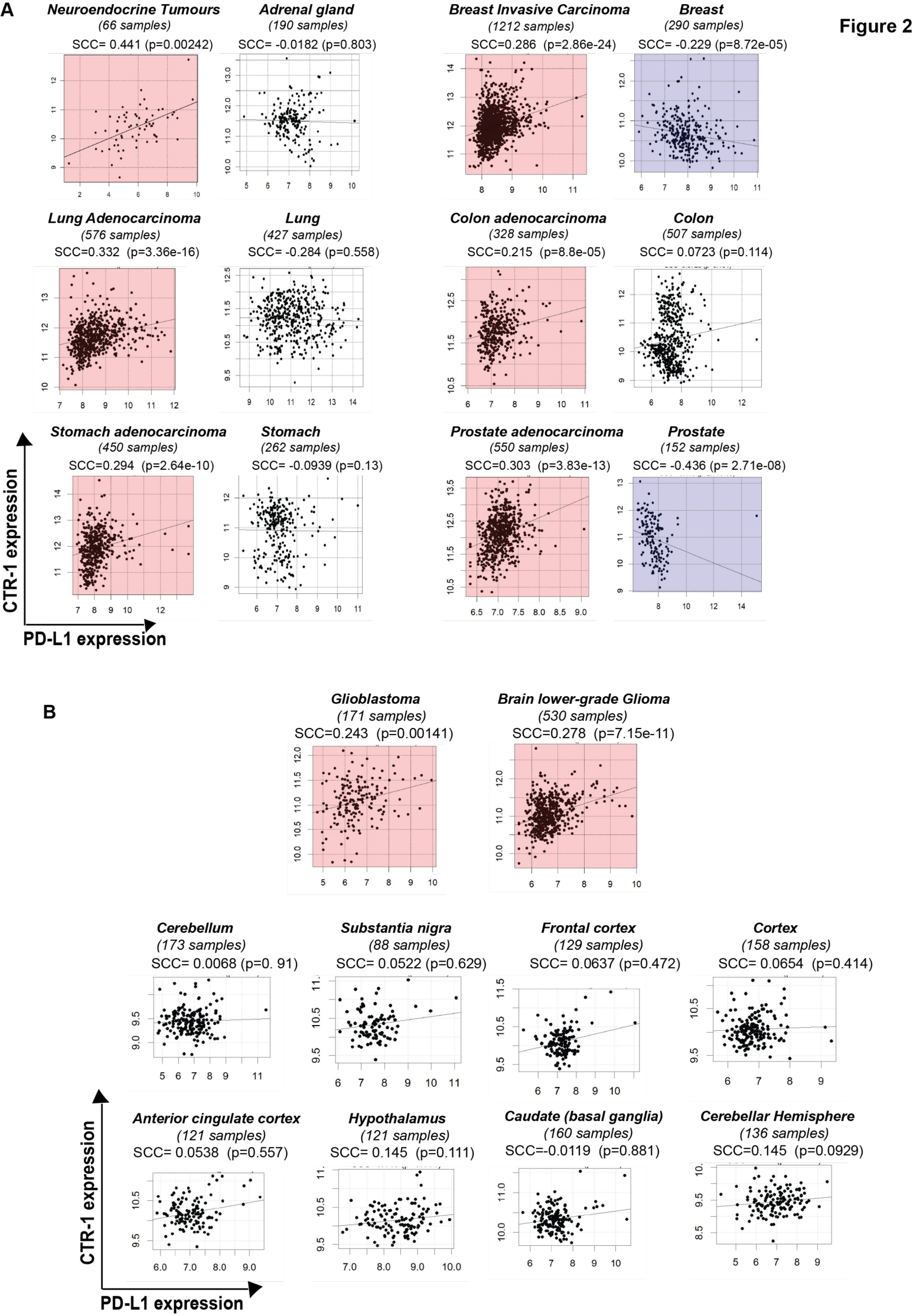
Figure 2
A
Neuroendocrine Tumours
(66 samples)
SCC= 0.441 (p=0.00242)
Adrenal gland
(190 samples)
SCC= -0.0182 (p=0.803)
Breast Invasive Carcinoma
(1212 samples)
SCC=0.286 (p=2.86e-24)
Breast
(290 samples)
SCC= -0.229 (p=8.72e-05)
Lung Adenocarcinoma
(576 samples)
SCC=0.332 (p=3.36e-16)
Lung
(427 samples)
SCC= -0.284 (p=0.558)
Colon adenocarcinoma
(328 samples)
SCC=0.215 (p=8.8e-05)
Colon
(507 samples)
SCC= 0.0723 (p=0.114)
Stomach adenocarcinoma
(450 samples)
SCC=0.294 (p=2.64e-10)
Stomach
(262 samples)
SCC= -0.0939 (p=0.13)
Prostate adenocarcinoma
(550 samples)
SCC=0.303 (p=3.83e-13)
Prostate
(152 samples)
SCC= -0.436 (p= 2.71e-08)
CTR-1 expression
PD-L1 expression
B
Glioblastoma
(171 samples)
SCC=0.243 (p=0.00141)
Brain lower-grade Glioma
(530 samples)
SCC=0.278 (p=7.15e-11)
Cerebellum
(173 samples)
SCC= 0.0068 (p=0. 91)
Substantia nigra
(88 samples)
SCC= 0.0522 (p=0.629)
Frontal cortex
(129 samples)
SCC= 0.0637 (p=0.472)
Cortex
(158 samples)
SCC= 0.0654 (p=0.414)
Anterior cingulate cortex
(121 samples)
SCC= 0.0538 (p=0.557)
Hypothalamus
(121 samples)
SCC= 0.145 (p=0.111)
Caudate (basal ganglia)
(160 samples)
SCC=-0.0119 (p=0.881)
Cerebellar Hemisphere
(136 samples)
SCC=0.145 (p=0.0929)
CTR-1 expression
PD-L1 expression

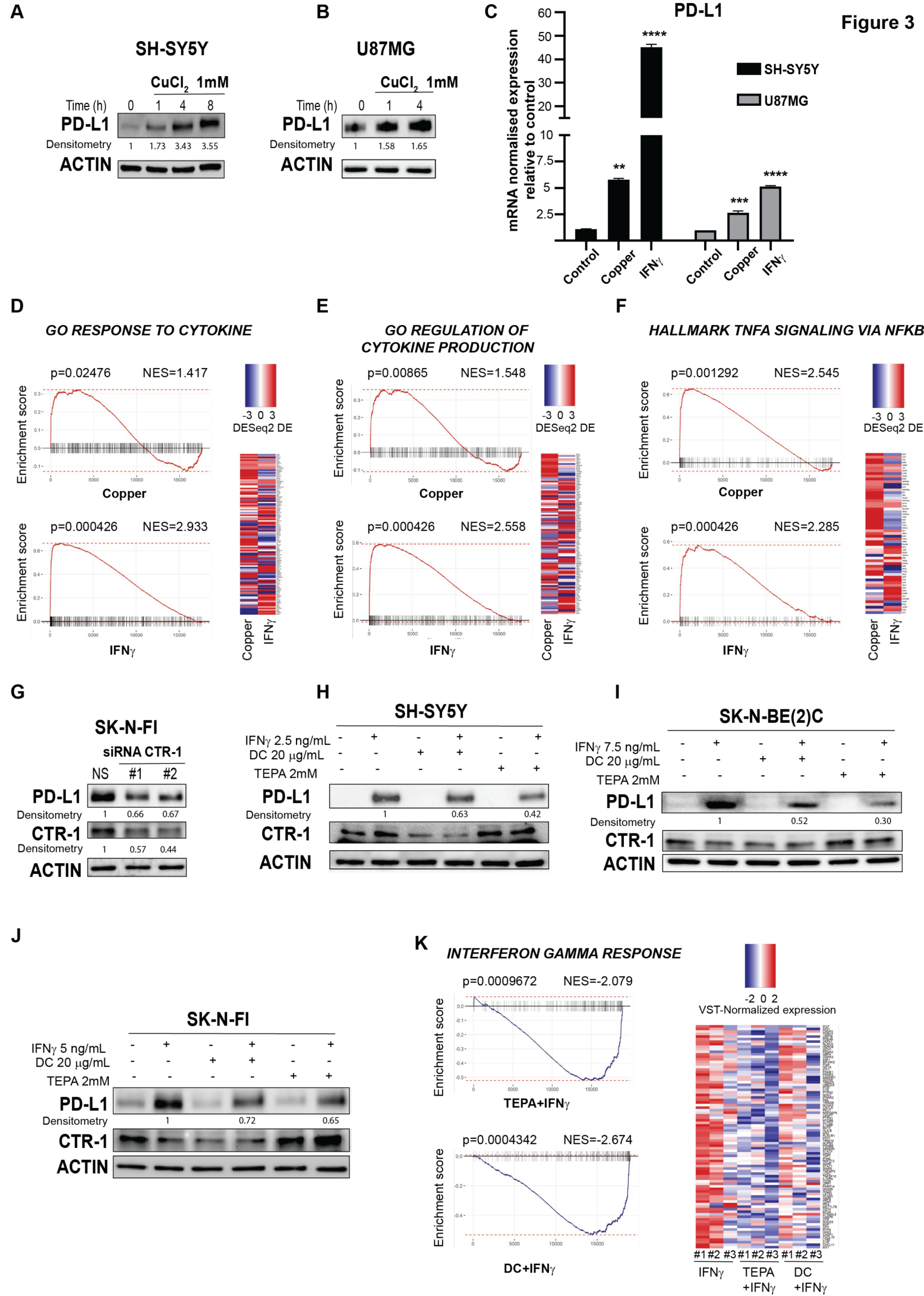
Figure 3
A
SH-SY5Y
CuCl2 1mM
Time (h) 0 1 4 8
PD-L1
Densitometry 1 1.73 3.43 3.55
ACTIN
B
U87MG
CuCl2 1mM
Time (h) 0 1 4
PD-L1
Densitometry 1 1.58 1.65
ACTIN
C
PD-L1
mRNA normalised expression relative to control
SH-SY5Y
U87MG
Control
Copper
IFNγ
D
GO RESPONSE TO CYTOKINE
p=0.02476 NES=1.417
p=0.000426 NES=2.933
Enrichment score
Copper
IFNγ
-3 0 3
DESeq2 DE
E
GO REGULATION OF CYTOKINE PRODUCTION
p=0.00865 NES=1.548
p=0.000426 NES=2.558
F
HALLMARK TNFA SIGNALING VIA NFKB
p=0.001292 NES=2.545
p=0.000426 NES=2.285
G
SK-N-FI
siRNA CTR-1
NS #1 #2
PD-L1
Densitometry 1 0.66 0.67
CTR-1
Densitometry 1 0.57 0.44
ACTIN
H
SH-SY5Y
IFNγ 2.5 ng/mL
DC 20 μg/mL
TEPA 2mM
PD-L1
Densitometry 1 0.63 0.42
CTR-1
ACTIN
I
SK-N-BE(2)C
IFNγ 7.5 ng/mL
DC 20 μg/mL
TEPA 2mM
PD-L1
Densitometry 1 0.52 0.30
CTR-1
ACTIN
J
SK-N-FI
IFNγ 5 ng/mL
DC 20 μg/mL
TEPA 2mM
PD-L1
Densitometry 1 0.72 0.65
CTR-1
ACTIN
K
INTERFERON GAMMA RESPONSE
p=0.0009672 NES=-2.079
TEPA+IFNγ
p=0.0004342 NES=-2.674
DC+IFNγ
-2 0 2
VST-Normalized expression
#1 #2 #3 #1 #2 #3 #1 #2 #3
IFNγ
TEPA +IFNγ
DC +IFNγ

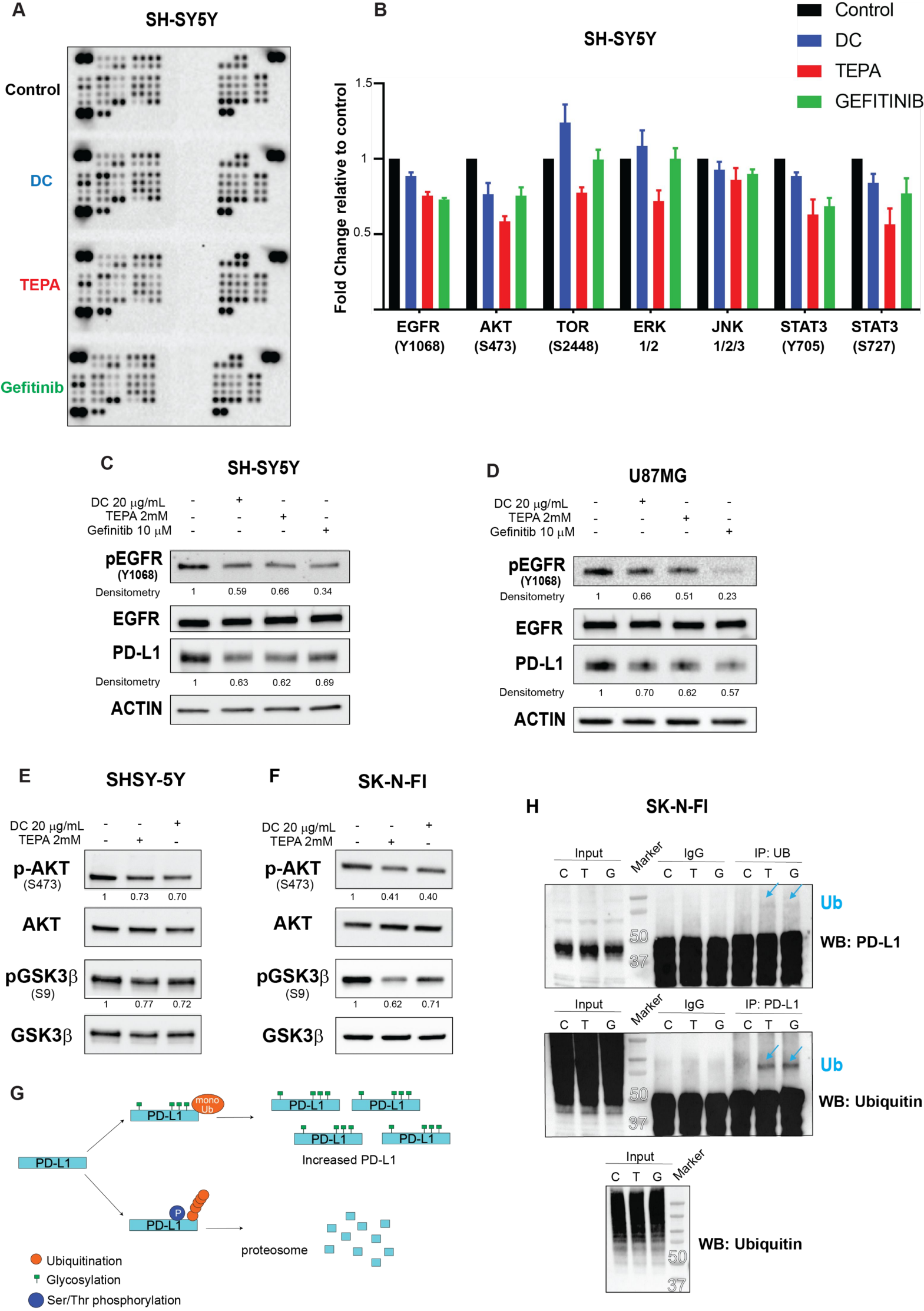
A
SH-SY5Y
Control
DC
TEPA
Gefitinib
B
SH-SY5Y
Control
DC
TEPA
GEFITINIB
Fold Change relative to control
1.5
1
0.5
EGFR (Y1068)
AKT (S473)
TOR (S2448)
ERK 1/2
JNK 1/2/3
STAT3 (Y705)
STAT3 (S727)
C
SH-SY5Y
DC 20 μg/mL - + - -
TEPA 2mM - - + -
Gefinitib 10 μM - - - +
pEGFR (Y1068)
Densitometry 1 0.59 0.66 0.34
EGFR
PD-L1
Densitometry 1 0.63 0.62 0.69
ACTIN
D
U87MG
DC 20 μg/mL - + - -
TEPA 2mM - - + -
Gefinitib 10 μM - - - +
pEGFR (Y1068)
Densitometry 1 0.66 0.51 0.23
EGFR
PD-L1
Densitometry 1 0.70 0.62 0.57
ACTIN
E
SHSY-5Y
DC 20 μg/mL - - +
TEPA 2mM - + -
p-AKT (S473)
1 0.73 0.70
AKT
pGSK3β (S9)
1 0.77 0.72
GSK3β
F
SK-N-FI
DC 20 μg/mL - - +
TEPA 2mM - + -
p-AKT (S473)
1 0.41 0.40
AKT
pGSK3β (S9)
1 0.62 0.71
GSK3β
H
SK-N-FI
Input
Marker
IgG
IP: UB
C T G
Ub
WB: PD-L1
50
37
IP: PD-L1
WB: Ubiquitin
G
PD-L1
mono Ub
Increased PD-L1
P
proteosome
Ubiquitination
Glycosylation
Ser/Thr phosphorylation

Figure 5

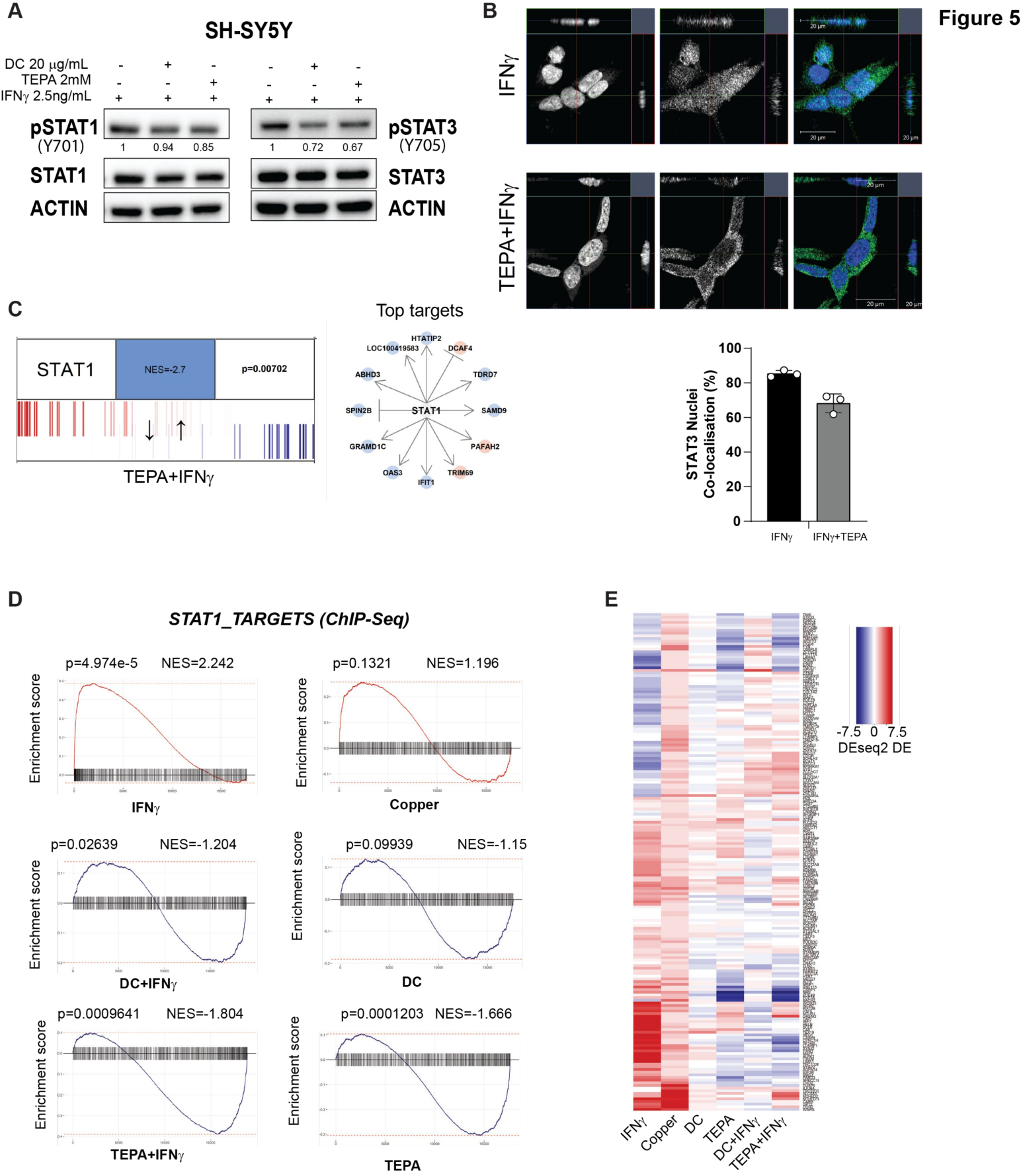
A
SH-SY5Y
DC 20 μg/mL
TEPA 2mM
IFNγ 2.5ng/mL
pSTAT1 (Y701)
1 0.94 0.85
1 0.72 0.67
pSTAT3 (Y705)
STAT1
STAT3
ACTIN
B
IFNγ
TEPA+IFNγ
20 μm
C
STAT1
NES=-2.7
p=0.00702
TEPA+IFNγ
Top targets
HTATIP2
LOC100419583
DCAF4
ABHD3
TDRD7
SPIN2B
STAT1
SAMD9
GRAMD1C
PAFAH2
OAS3
TRIM69
IFIT1
STAT3 Nuclei Co-localisation (%)
IFNγ
IFNγ+TEPA
D
STAT1_TARGETS (ChIP-Seq)
p=4.974e-5 NES=2.242
IFNγ
p=0.1321 NES=1.196
Copper
p=0.02639 NES=-1.204
DC+IFNγ
p=0.09939 NES=-1.15
DC
p=0.0009641 NES=-1.804
TEPA+IFNγ
p=0.0001203 NES=-1.666
TEPA
Enrichment score
E
-7.5 0 7.5
DEseq2 DE
IFNγ
Copper
DC
TEPA
DC+IFNγ
TEPA+IFNγ

Figure 6

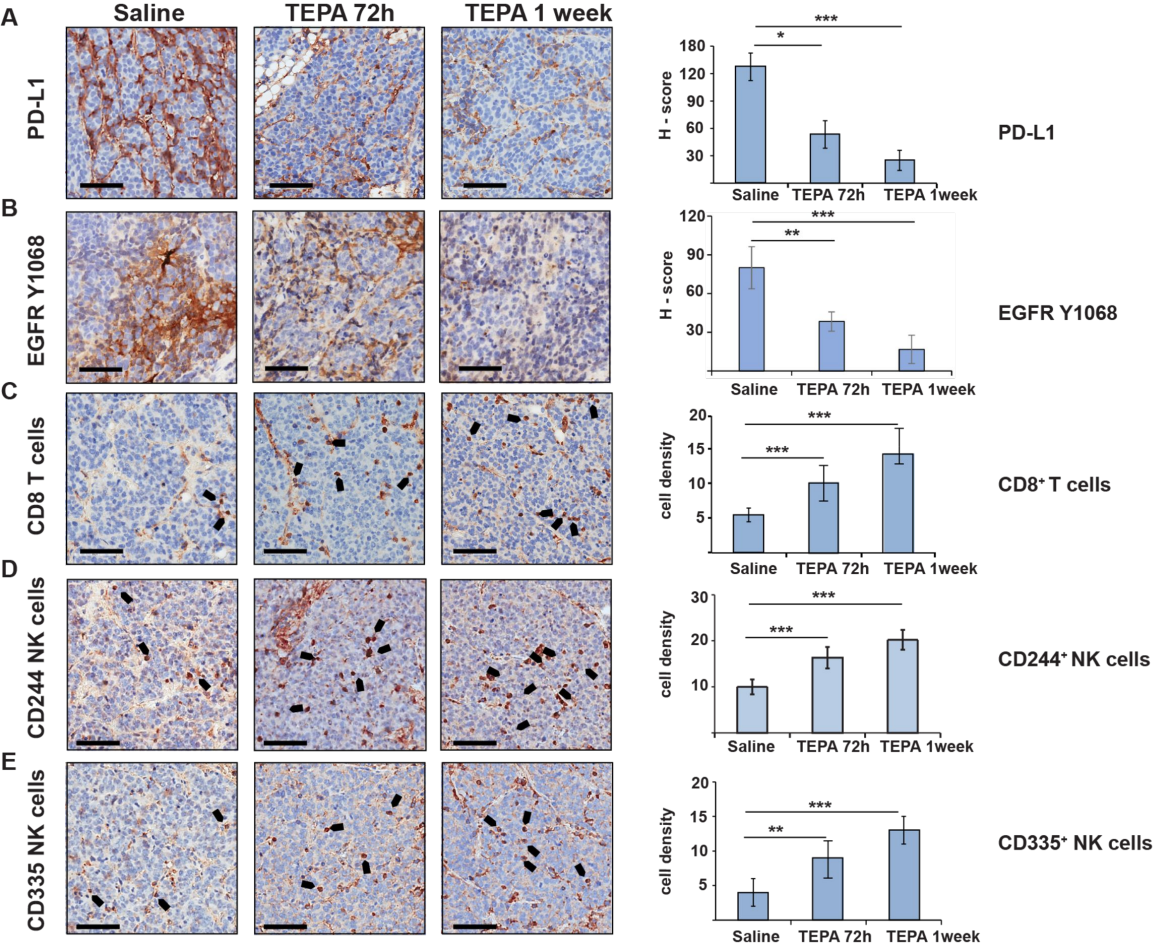
A
Saline
TEPA 72h
TEPA 1 week
PD-L1
H - score
Saline
TEPA 72h
TEPA 1week
B
EGFR Y1068
C
CD8 T cells
cell density
CD8⁺ T cells
D
CD244 NK cells
CD244⁺ NK cells
E
CD335 NK cells
CD335⁺ NK cells

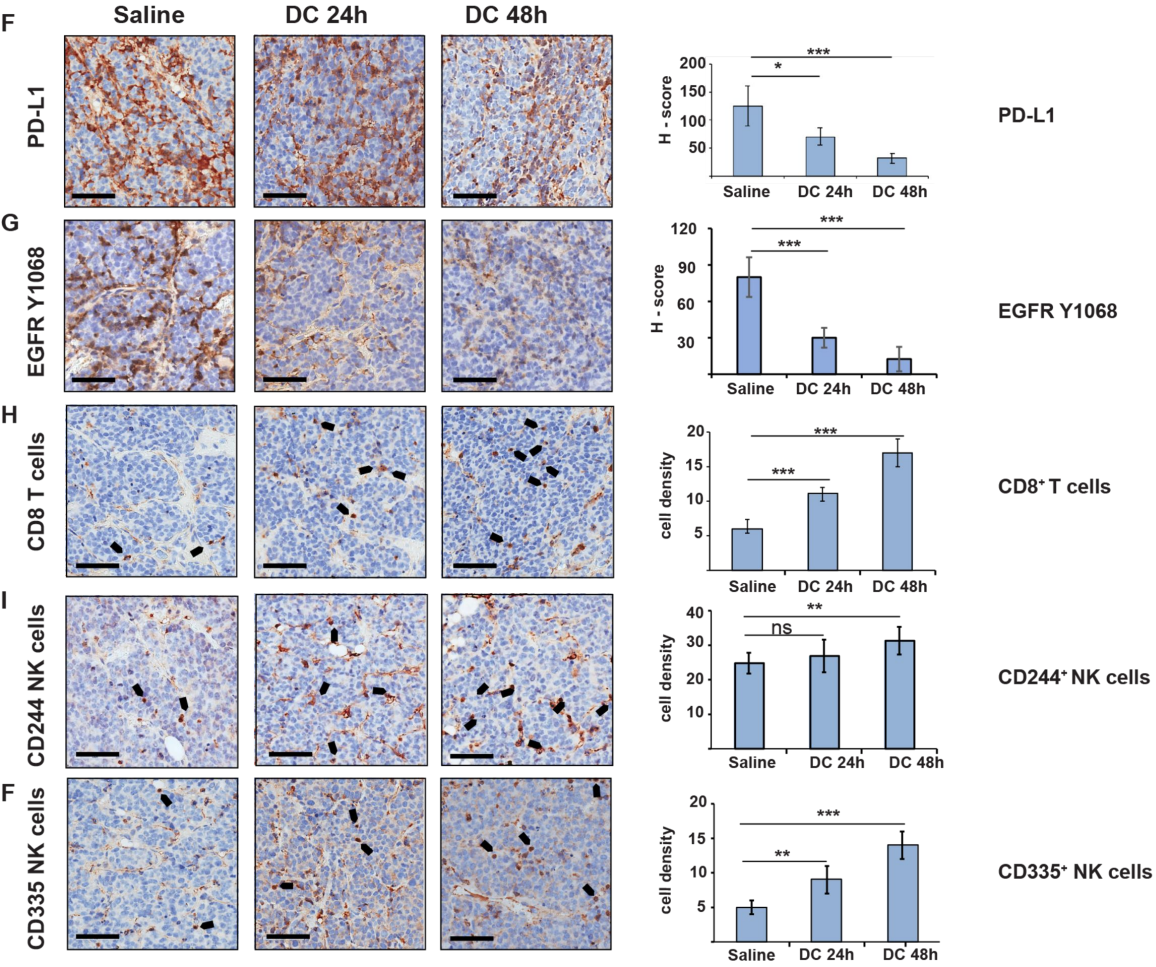
F
Saline
DC 24h
DC 48h
PD-L1
H - score
G
EGFR Y1068
H
CD8 T cells
cell density
CD8⁺ T cells
I
CD244 NK cells
ns
CD244⁺ NK cells
F
CD335 NK cells
CD335⁺ NK cells

Figure 7

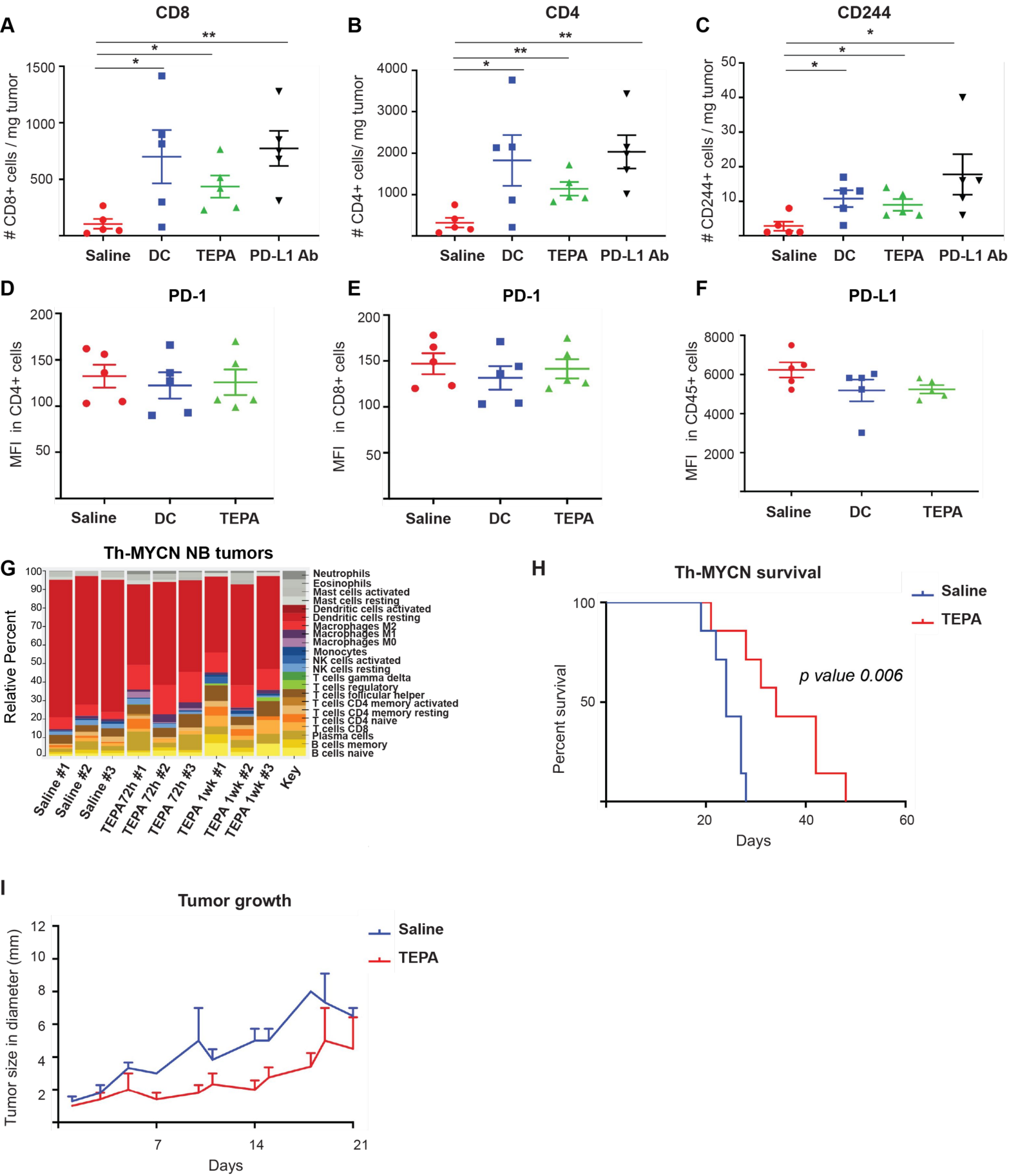
A
CD8
CD8+ cells / mg tumor
1500
1000
500
Saline
DC
TEPA
PD-L1 Ab
B
CD4
CD4+ cells/ mg tumor
4000
3000
2000
1000
C
CD244
CD244+ cells / mg tumor
50
40
30
20
10
D
PD-1
MFI in CD4+ cells
200
150
100
50
E
PD-1
MFI in CD8+ cells
F
PD-L1
MFI in CD45+ cells
8000
6000
4000
2000
G
Th-MYCN NB tumors
Relative Percent
Neutrophils
Eosinophils
Mast cells activated
Mast cells resting
Dendritic cells activated
Dendritic cells resting
Macrophages M2
Macrophages M1
Macrophages M0
Monocytes
NK cells activated
NK cells resting
T cells gamma delta
T cells regulatory
T cells follicular helper
T cells CD4 memory activated
T cells CD4 memory resting
T cells CD4 naive
T cells CD8
Plasma cells
B cells memory
B cells naive
Saline #1
Saline #2
Saline #3
TEPA72h #1
TEPA 72h #2
TEPA 72h #3
TEPA 1wk #1
TEPA 1wk #2
TEPA 1wk #3
Key
H
Th-MYCN survival
Saline
TEPA
p value 0.006
Percent survival
Days
I
Tumor growth
Tumor size in diameter (mm)
Days